Electromagnetic analysis of conducting and plasmonic scatterers using theory of characteristic modes

Joni Lappalainen

School of Electrical Engineering

Thesis submitted for examination for the degree of Master of Science in Technology.

Espoo 13.3.2017

Thesis supervisor:

Prof. Ari Sihvola

Thesis advisor:

Docent Pasi Ylä-Oijala

Aalto University
School of Electrical
Engineering

AALTO UNIVERSITY
SCHOOL OF ELECTRICAL ENGINEERING

ABSTRACT OF THE
MASTER'S THESIS

Author: Joni Lappalainen

Title: Electromagnetic analysis of conducting and plasmonic scatterers using theory of characteristic modes

Date: 13.3.2017 Language: English Number of pages: 7+44

Department of Nano and Radio sciences

Professorship: Radio Science and Engineering

Supervisor: Prof. Ari Sihvola

Advisor: Docent Pasi Ylä-Oijala

The goal of this work was to show how Theory of Characteristic Modes can be used in the characterization of electromagnetic scatterers as well as introduce and formulate a new surface integral equation applicable for modal analysis of multi-layered scatterers.

To be able to do this, in this work the problem under inspection is shortly introduced and the reader is then familiarized with the mathematical, physical and numerical basis of surface equivalence representations. Some numerical examples are also introduced, which exist to illustrate the benefit of modal analysis and are also used to validate the new formulation via comparison to analytical solutions.

In the end a working formulation to be used in the modal analysis of multi-layered scatterers was found via a systematic application of known theories. The formulations allows also further development and generalization of surface integral representations.

Keywords: Electromagnetic scattering, Computational electromagnetics, Theory of Characteristic Modes, Surface integral equations

AALTO-YLIOPISTO
SÄHKÖTEKNIIKAN KORKEAKOULU

DIPLOMITYÖN
TIIVISTELMÄ

Tekijä: Joni Lappalainen

Työn nimi: Karakteristisiten moodien käyttö johtavien ja plasmonisten sirottajien analysoinnissa

Päivämäärä: 13.3.2017 Kieli: Englanti Sivumäärä: 7+44

Radiotieteen ja -tekniikan laitos

Professuuri: Radiotiede- ja tekniikka

Työn valvoja: Prof. Ari Sihvola

Työn ohjaaja: Dos. Pasi Ylä-Oijala

Tämän työn tavoitteena oli esitellä karakteristisiten moodien teorian käyttöä sirontaongelmien analysoinnissa. Tämän lisäksi työn tavoitteena oli esitellä ja muodostaa uusi moodianalyysin salliva integraaliyhtälöesitys monikerrosrakenteille.

Tämän mahdollistamiseksi työssä esitellään geneerisen sirontehtävän taustateoria lyhyesti, jonka jälkeen lukija perehdytetään pintaekvivalenssiperiaatteen fyysiseen, matemaattiseen ja numeeriseen perustaan. Työssä esitellään myös numeerisia tuloksia, joilla korostetaan mooditeorian hyötyjä sekä valitoidaan uusi formulaatio.

Työn aikana monikerrosongelmien moodianalyysissa toimiva formulaatio saatiin muodostettua ja validoitua varsin suoraviivaisesti soveltamalla hyvin tunnettuja, aiempia teorioita. Samalla huomattiin, että uusi ratkaisu kyetään yleistämään ja/tai soveltamaan varsin suoraviivaisesti myös monimutkaisempiin ongelmiin.

Avainsanat: Sähkömagnetiikan sirontatehtävä, Laskennallinen sähkömagnetiikka, Karakteristiset moodit, Pintaintegraalimenetelmät

Preface

This thesis wouldn't exist without the research already carried out at the Department of Electronics and Nanoengineering of Aalto University of Electrical Engineering. I'd also like to thank the following personnel for making this thesis possible.

First of all, naturally, I'd like to thank all the professors and assistants with whom I've had the privilege to work with, and more than anything, *learn from*.

I'd also like to thank the all the members of the Electromagnetics group: advisor Docent Pasi Ylä-Oijala for his seemingly infinite patience – most certainly needed in guiding an engineer of applied sciences through a field of mathematics. Supervisor Prof. Ari Sihvola for his kindness, guidance and optimism in my skills and Dimitrios Tzarouchis for having motivated me to embark on this journey in the first place.

Worth thanking for is more or less the whole group of Antennas and Wireless Sensors, having provided me shoulders to cry on and discussions to keep my feet on the ground and eyes on applications.

Last but not least I'd like to thank my friends and family for their everlasting support, especially my beautiful and loving wife Ida, who despite all my stress, uncertainty and hustle has never stopped believing in or failed in soothing me down and provided us the most perfect baby girl in the world.

Otaniemi, 13.3.2017

Joni E. S. Lappalainen

Contents

Abstract ii

Abstract (in Finnish) iii

Preface iv

Contents v

Symbols and abbreviations vi

1 Introduction 1

2 Problem statement 3
2.1 Scattering problem . . . 3
2.2 Maxwell's equations and boundary conditions . . . 5
2.3 Integral equation representation . . . 6
2.4 Electromagnetic materials . . . 8

3 Theoretical formulations 10
3.1 Perfect electric conductors . . . 12
3.2 Penetrable objects . . . 14
3.3 Core-shell structures . . . 16

4 Numerical solutions 23
4.1 Weak formulation . . . 23
4.2 Basis functions and testing . . . 24
4.3 Extraction of results . . . 27

5 Numerical results 30
5.1 Perfect electric conductors . . . 30
5.2 Plasmonic nanoparticles . . . 33
5.3 Core-shell structures . . . 36

6 Conclusions 40

References 41

Symbols and abbreviations

Symbols

$\mathbf{E}$	electric field
$\mathbf{H}$	magnetic field
$\mathbf{B}$	magnetic flux density
$\mathbf{D}$	electric flux density
ϵ	electric permittivity
ϵ_r	relative permittivity
μ	magnetic permeability
μ_r	relative permeability
ϵ_0	permittivity of free space $\approx 8.854 \times 10^{-12}$ [F/m]
$\mathbf{A}_{tan}$	tangential component of field A
$\mathbf{n} \cdot \mathbf{A}$	normal component of field A
$\bar{\bar{\mathcal{Z}}}_S$	surface impedance (dyadic)
c	speed of light $\approx 3 \times 10^8$ [m/s]
η	wave impedance
k	wavenumber
Z	impedance, $R + iX$
i	imaginary unit
R	resistance, $\Re e(Z)$
X	reactance, $\Im m(Z)$
I	identity matrix

Operators

$\nabla \times \mathbf{A}$	curl of vector $\mathbf{A}$
$\int_\Omega \mathbf{A}\, d\Omega$	integral of $\mathbf{A}$ over domain Ω
δ_{j0}	Kroenecker delta
$\nabla_S \cdot$	surface divergence
$\sum_j$	sum over index j
$\mathbf{A} \cdot \mathbf{B}$	dot product of vectors $\mathbf{A}$ and $\mathbf{B}$
$\mathbf{A}^*$	complex conjugate of $\mathbf{A}$
$\Re e[\mathbf{A}]$	real part of $\mathbf{A}$
$\Im m[\mathbf{A}]$	imaginary part of $\mathbf{A}$
χ_j	characteristic function of domain Ω_j
G	Green's function
$\gamma_t \mathbf{F}$	tangential trace operator
$\gamma_r \mathbf{F}$	rotated tangential trace operator
$< \mathbf{a}, \mathbf{b} >_S$	integral of $\mathbf{a} \cdot \mathbf{b}$ over S, i.e., $\int \mathbf{a} \cdot \mathbf{b}\, dS$
$\dfrac{\mathrm{d}}{\mathrm{d}t}$	derivative with respect to variable t
$\dfrac{\partial}{\partial t}$	partial derivative with respect to variable t

Abbreviations

BC	Buffa–Christiansen
CFIE	combined field integral equation
CM	characteristic mode
DC	direct current
DOF	degree(s) of freedom
EFIE	electric field integral equation
EM	electromagnetic
FEM	finite element method
IBC	impedance boundary condition
LHS	left-hand side of equation
MFIE	magnetic field integral equation
PDE	partial differential equation
PEC	perfect electric conductor
RHS	right-hand side of equation
RWG	Rao–Wilton–Glisson
SEP	surface equivalence principle
SIE	surface integral equation
TCM	theory of characteristic modes
TEM	transverse eletromagnetic

1 Introduction

Theory of characteristic modes (TCM) isn't actually a new field of study: for instance the purely analytical modal expansion technique for infinite waveguides is a rather well-known and exploited solution in the field of *electromagnetics* (EM). However as the capabilities in terms of memory and processor speeds has drastically increased for computers, old mathematical theories have found new meanings in the multidisciplinary field of *computational electromagnetics* (CEM), allowing the search for solutions even for geometries not possessing analytical solutions.

This property is especially sought after in *antenna engineering*, as often the geometry is not a pure degree of freedom, but is instead strictly bounded in both shape and size arising from manufacturing or other application dependent needs. Also, as one of the main properties of TCM is *excitation independency* and ability to express solutions via *orthogonal modes*, in the era of arising 5G, i.e, extremely high frequency technologies, tackling problems like mutual coupling is no longer trivial. [1] Additionally TCM has lately been emerging in to the characterization of *plasmonic* objects, i.e., metal objects with nano-scale dimensions at optical regime, where the free electrons no longer act as an impenetrable boundary, but instead allow for negative permittivities and provide, for instance, rather interesting wave-guiding possibilities for sub-wavelength scatterers.

A great variety of numerical models exist, upon which scattering formulations can be built upon. However, as antenna and *scattering* problems are highly dependent on *far field properties*, many of the available schemes, like *finite element method* (FEM) and *finite-difference time-domain* method (FDTD) result to large computational domains. *Surface integral equation* formulations avoid this problem, as they are able to represent an original problem in a 3D domain by equivalent sources on a 2D surface via *surface equivalence principle* (SEP), often greatly lowering the required computational resources in representing an antenna or scattering problem numerically.

However, the amount of available SIE formulations for TCM is still quite limited, for instance, not allowing for the representation multi-layered structures, i.e, any object, that has a material completely enclosed by another material. Thus, the main aim of this work is to be able to formulate and implement a new numerical *surface integral equation* (SIE) TCM formulation for multi-layered structures. To that end I have to familiarize myself with the already existing integral equation representations, starting from the simplest and well known *electric field integral equation* (EFIE) towards the objectives of this work. To be able to implement the method and evaluate the obtained results, I also had to familiarize myself with the core of numerical methods like *weak formulation* and *basis functions*.

This thesis is organized as follows. In Chapter 2 the problem under inspection and its governing theory as well as integral equation representations are described and discussion on materials is presented. In Chapter 3 TCM and its properties are discussed and a wide variety of integral equation formulations for both scattering and characteristic mode problems are formulated, including the new one for multi-layered structures. Also some motivation via their applications are introduced. Chapter

4 then briefly describes how numerical schemes can be built upon the introduced formulations. In Chapter 5 examples of using TCM in the characterization of scatterers are shown and the validity of the new method is ensured via comparison to analytical solutions. This work ends in Chapter 6, where conclusion are drawn and topics of future work are discussed.

2 Problem statement

In this chapter we introduce the problem under inspection, its governing theory and the resulting mathematical equations. We'll also introduce a field, in which this problem is currently rather relevant, namely *plasmonics*.

2.1 Scattering problem

We're set to solve a rather fundamental electromagnetic (EM) problem: if an object is placed in a primary electromagnetic field, what will be the effect of the field on the object, *scatterer*, and what will be its response? In Figure 1 these *primary* and *scattered fields* are denoted correspondingly $\mathbf{E}^p$ and $\mathbf{E}^s$. This is an example of a simple *scattering problem* and it is of utmost interest, as its results describe the interaction of electromagnetic waves with material. The solutions of scattering problems are used do develop understanding on a great variety of designs going from radars to antennas and even fundamental physics, like Raman scattering and generation of photons.

As an example, a simple one-body scattering problem is introduced here: a single object is placed in an unbounded domain Ω_0, Ω_1 then being the domain bounded by the surface of the object, denoted by S. The total fields in both domains can be expressed according to the *superposition principle* as a sum of the primary and secondary fields as

$$\mathbf{E}_0 = \mathbf{E}_0^p + \mathbf{E}_0^s \tag{1a}$$
$$\mathbf{E}_1 = \mathbf{E}_1^s \tag{1b}$$
$$\mathbf{H}_0 = \mathbf{H}_0^p + \mathbf{H}_0^s \tag{1c}$$
$$\mathbf{H}_1 = \mathbf{H}_1^s. \tag{1d}$$

where the subscript is used to denote in which domain the fields are represented in and $\mathbf{H}_j, j = 0, 1$, is the magnetic field.

In EM problems the *cross sections* are often used as figures of merit. The scattering cross section, σ_{sca}, is defined as the energy stored in the scattered field versus the power density of the incident field, i.e., it describes the ability of the scatterer to perturbate the incident field. The *absorption cross section*, σ_{abs}, is the ratio of the total absorbed power inside the scatterer over the incident power density, i.e., it describes the ability of the scatterer to absorb energy from the incident field. As equations these are given by

$$\sigma_{sca} = \frac{P_{sca}}{|\mathbf{S}|} \tag{2a}$$
$$\sigma_{abs} = \frac{P_{abs}}{|\mathbf{S}|} \tag{2b}$$

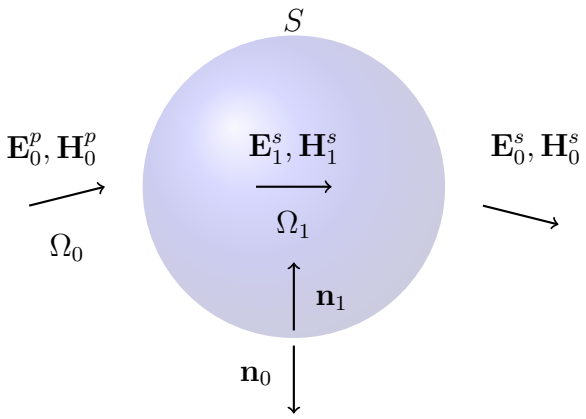

Figure 1: One-body scattering problem

where $\mathbf{S}$ is the incident power density illuminating the object and the absorbed and scattered powers are obtained from

$$P_{sca} = \int_S \frac{1}{2}\mathfrak{Re}[\mathbf{E}_0^s \times \mathbf{H}_0^{s*}] \cdot \mathbf{n}\, dS \tag{3a}$$

$$P_{abs} = -\int_S \frac{1}{2}\mathfrak{Re}[\mathbf{E}_0 \times \mathbf{H}_0^{*}] \cdot \mathbf{n}\, dS. \tag{3b}$$

where S is any closed surface, that encloses the scatterer.

In solving a special case of scattering, an *antenna* problem, also the *radiation patterns* and *polarizations*, shown in Figure 2, are used in describing the behaviour of the scatterer. They describe how the field is distributed and thus propagate in the 3D-domain and in which plane the field vectors lie in. These affect the possible communication directions and polarisations, i.e., the possible excitations, on which the scatterer, antenna is able to accept and thus send energy. These are practically always defined in the *far field*, electrically far enough from the antenna that the antenna pattern has become stable and can be approximated as a *plane wave* locally.

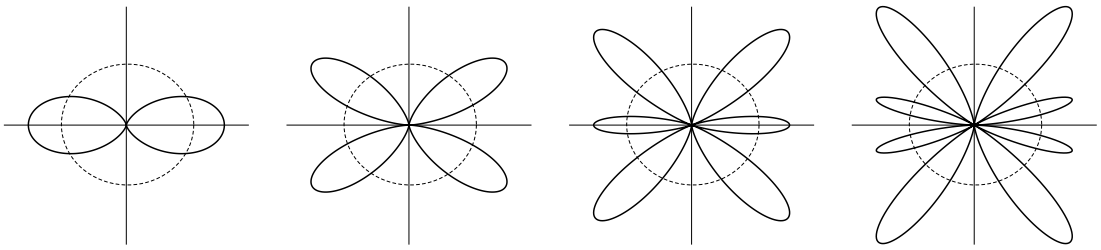

Figure 2: Far field radiation patterns (from left to right) for a dipole, quadrupole, hexapole, and octopole

Even though introduced here for one scatterer in a simple background medium, this approach is valid for n objects, some of which might be inside each other, known

as *core-shell structures*. If we're willing to solve the scattering problem, we now have a system of equations that is underdefined: we know only the primary fields, not total nor scattered. Thus we need to link the unknown quantities to the known ones through the *Maxwell's equations*.

2.2 Maxwell's equations and boundary conditions

It was shown in the 19th-century, that electromagnetic radiation fulfils the *Maxwell's equations* of which there exists both time and frequency domain formulations. Here, due to the nature of our problem, we assume *time harmonic* evolution of the fields and currents: their time dependence is of the form $e^{-i\omega t}$, which allows us to replace a time derivative $\partial/\partial t$ with $-i\omega$. If we also assume a passive and thus *source free region*, the time harmonic Maxwell's equations become

$$\nabla \times \mathbf{E} = \quad i\omega\mathbf{B} \tag{4a}$$
$$\nabla \times \mathbf{H} = -i\omega\mathbf{D} \tag{4b}$$
$$\nabla \cdot \mathbf{D} = 0 \tag{4c}$$
$$\nabla \cdot \mathbf{B} = 0 \tag{4d}$$

where $\mathbf{D}$ and $\mathbf{B}$ are electric and magnetic fluxes, which are in a linear and direction independent , i.e., isotropic medium related to the electric and magnetic field quantities as

$$\mathbf{D} = \epsilon_j \mathbf{E} \tag{5a}$$
$$\mathbf{B} = \mu_j \mathbf{H} \tag{5b}$$

in which ϵ_j and μ_j are the electric permittivity and magnetic permeability of domain Ω_j respectively, however generally μ_0 and ϵ_0 then referring to *free space parameters*.

On an interface between two media with different EM properties (ϵ and/or μ) the solution should only fulfil also the *boundary* or *interface conditions*: across an interface of two linear and source free media the following field components

$$\mathbf{E}_{tan},\ \mathbf{H}_{tan},\ \mathbf{n}\cdot\mathbf{D} \ \text{ and } \ \mathbf{n}\cdot\mathbf{B} \tag{6}$$

should be continuous. Here $\mathbf{n}$ denotes the surface normal of boundary S and $\mathbf{A}_{tan}$ the component of a vector tangential to that surface. If the material is perfectly conducting (PEC), i.e., non-penetrable, any voltage difference along the surface will immediately be driven to zero as is the field, resulting in

$$\mathbf{E}_{tan} = 0,\ \mathbf{n}\cdot\mathbf{B} = 0. \tag{7}$$

For a non ideal conductor the *impedance boundary condition* (IBC) can be used, given as

$$\mathbf{E}_{tan} = \bar{\bar{\mathcal{Z}}}_S \cdot (\mathbf{n} \times \mathbf{H}) \tag{8}$$

where $\bar{\bar{\mathcal{Z}}}_S$ is the surface impedance dyadic, describing the relation between tangential electric field and rotated tangential magnetic field. IBC should approach the PEC boundary condition as $\bar{\bar{\mathcal{Z}}}_S \to 0$ [2]. As this work is focused in the analysis of PEC and plasmonic, i.e., penetrable scatterers, IBC is not further discussed but only introduced for the readers' curiosity.

Even though not a boundary condition as such, the scattered fields must also fulfil the radiation condition: the energy should diminish as $\mathbf{r} \to \infty$, i.e., the scattered energy must remain finite. The following being a peculiarity and not to be pondered upon too much, but the plane wave does not itself fulfil the radiation condition, having infinite energy. This is as a plane wave is but as an approximation of a field, the source of which is far away and stays quasi-constant over the computational area of interest.

2.3 Integral equation representation

Utilizing *equivalence principles*, a scattering problem is turned to an equivalent problem, in which the scatterer is replaced by equivalent sources that are able to reproduce the EM radiation of the original problem. The resulting formulations are known as *integral equation representations*.

If a surface S encloses a homogeneous and isotropic domain with constant and scalar material parameters ϵ and μ and the primary sources $\mathbf{E}^p$ and $\mathbf{H}^p$ are inside that domain, then according to the *surface equivalence principle* (SEP) the total fields inside the domain are uniquely defined by *equivalent surface current densities*

$$\mathbf{J}_S = \quad \mathbf{n} \times \mathbf{H} \tag{9a}$$
$$\mathbf{M}_S = -\mathbf{n} \times \mathbf{E}. \tag{9b}$$

where $\mathbf{J}_S$ is an equivalent electric and $\mathbf{M}_S$ magnetic current defined on the surface S. It is important to note, that they do not generally agree to any physical currents but are a *Huygens' principle* like representation of the original problem. [3]

Using the surface equivalence principle to the scattering problem defined in Figure 1 gives us the equivalent problems shown in Figure 3. In forming SEP for a problem the boundary between the domains separated by a surface is removed, i.e., material parameters are unified and sources outside that domain are set to zero, as they are already represented by the equivalent currents. This is accomplished with the help of a *characteristic function* of the corresponding domain Ω_j, χ_j defined as:

$$\chi_0 = \begin{cases} 1, & \mathbf{r} \in \Omega_0 \\ \dfrac{1}{2}, & \mathbf{r} \in S \\ 0, & \mathbf{r} \in \Omega_1 \end{cases} \tag{10a}$$

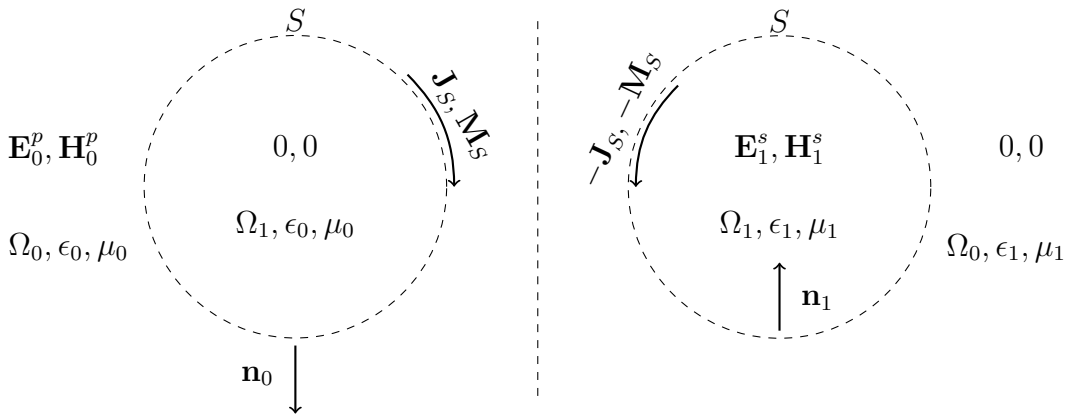

Figure 3: Surface equivalence representation of a simple scattering problem for domain Ω_0 (left) and domain Ω_1 (right).

$$\chi_1 = 1 - \chi_0. \tag{10b}$$

Then the EM field in the domain is expressed through currents as

$$\chi_j \mathbf{E}_j = \eta_j \mathcal{T}_j[\mathbf{J}_S] - \mathcal{K}_j[\mathbf{M}_S] + \delta_{j0}\mathbf{E}^p \tag{11a}$$

$$\chi_j \mathbf{H}_j = \frac{1}{\eta_j}\,\mathcal{T}_j[\mathbf{M}_S] + \mathcal{K}_j[\mathbf{J}_S] + \delta_{j0}\mathbf{H}^p \tag{11b}$$

$$j \in [0, 1],$$

in which η_j is the wave impedance, defined as $\sqrt{\frac{\mu_j}{\epsilon_j}}$, δ_{j0} is the Kroenecker delta

$$\delta_{j0} = \begin{cases} 1, & \text{if } j = 0, \\ 0, & \text{if } j \neq 0. \end{cases} \tag{12}$$

and $\mathcal{T}_j$ and $\mathcal{K}_j$ are surface integral operators that are defined through a single layer operator $\mathcal{S}_j$ as

$$\mathcal{T}_j[\mathbf{F}](\mathbf{r}) := \frac{-1}{ik_j}\nabla\mathcal{S}_j[\nabla_S \cdot \mathbf{F}](\mathbf{r}) + ik_j\,\mathcal{S}_j[\mathbf{F}](\mathbf{r}) \tag{13a}$$

$$\mathcal{K}_j[\mathbf{F}](\mathbf{r}) := \nabla \times \mathcal{S}_j[\mathbf{F}](\mathbf{r}) \tag{13b}$$

$$\mathcal{S}_j[\mathbf{F}](\mathbf{r}) \;\; = \int_S G_j(\mathbf{r},\mathbf{r}')\mathbf{F}(\mathbf{r}')\,dS' \tag{13c}$$

where k_j is the wavenumber, defined as $k_j = \omega\sqrt{\epsilon_j\mu_j}$, $\nabla_S\cdot$ is the *surface divergence*, i.e., a divergence, from which the component normal to the surface is subtracted and G_j is the homogeneous free space Green's function, which is of the form

$$G_j(\mathbf{r}, \mathbf{r}') = \frac{e^{ik_j|\mathbf{r}\text{-}\mathbf{r}'|}}{4\pi|\mathbf{r}\text{-}\mathbf{r}'|}. \tag{14}$$

It is of worth noting that $\mathcal{T}_j$, $\mathcal{K}_j$ and $\mathcal{S}_j$ should operate on smooth enough vector functions for a solution to exist.

We now have a set of equations that is able to represent the problem only through the primary field components and boundary conditions , i.e., material dependent parameters. Thus next we'll discuss about the effect of material and introduce an important material model.

2.4 Electromagnetic materials

As seen from Equation (11), the permittivity and permeability of the scatterer, ϵ and μ, play a significant role in its EM response. They depict the material's ability to *polarize*, and also the penetration properties of a field, **E** or **H**, into the material. Majority of classical materials can be classified as

- isotropic: their parameters are direction independent.
- non-magnetic: their relative permeability, $\mu_r = \mu/\mu_0$ is 1.
- or can be represented as (piecewise) homogeneous: their parameters are (piecewise) constants.
- having relative permittivities, $\epsilon_r = \epsilon/\epsilon_0$, varying from 1 (free space) to ∞ (PEC).

In this work we focus on formulations for linear, isotropic and homogeneous scatterers, as the complexity of the formulations and computational effort of solutions quickly rises with complex materials that require proper Green's functions. However we do allow a single exception: we consider also *plasmonic materials*, which may exhibit negative permittivities, usually in the visible spectrum of EM radiation.

Plasmonics is a field studying and describing the electron-density oscillations sustained for example by semiconductor channels, thinmetal films and metal nanoparticles, and can for instance explain the optical properties of metals. Plasmonics is hardly a new field: in classical calculations the *surface plasmon* was foreseen already in the Mie-theory over a hundred years ago, and first experiments validating their existence by Ruthemann and Lang were made in the mid 20th-century. However recent advancements in nanofabrification have allowed a higher degree of freedom regarding the size and shape of produced nanoparticles and thus a need for tools that can accurately predict the properties of these particles has arisen.

In classical EM, plasmonic problems can be modelled as a special case of scattering. The oscillating behaviour of electrons can be described in the macro scale as a frequency varying permittivity of a metal particle, as the electron inertia and finite mobility result to a non-PEC response. The resulting material properties are then usually approximated with the *Drude model*. In the Drude model it is assumed that

the electrons of a metal cluster form an ideal electron gas, in which electrons can only interact via collisions - no forces between neighbouring electrons or nucleus exist, nor the nucleus is allowed to move. This results in a frequency dependent permittivity of the metal cluster, given as

$$\epsilon(\omega) = \epsilon_{\text{inf}} - \frac{\omega_p^2}{\omega(\omega + i\gamma)} \tag{15}$$

where ϵ_{inf} is the limit for permittivity as frequency approaches infinity, ω_p the so-called plasma frequency of the given material, and γ the intraband tracking term, inverse of the relaxation time. [4] As can be seen, the intraband tracking term gives rise to the imaginary part, which will result in a real propagation exponent, i.e., attenuation of the EM waves.

In this work all penetrable objects are assumed to be silver, Drude model parameters of which have been obtained from [5]. It is well known, that Drude models tend to underestimate the losses, i.e., the imaginary part of a scatterers permittivity, as the wavelength approaches 300 nm. As this mainly affects the quality factor, the results obtained with a Drude model are qualitatively accurate and widely used. Also, as the material model is formulation independent and can easily be switched if needed, further on in this work we assume our material model to be accurate enough.

Next we'll move from the general background a bit closer to the essence of this work: how *surface integral equations* (SIEs) and *characteristic mode* (CM) formulations can be developed for the introduced materials.

3 Theoretical formulations

In this section we review and replicate well-known SIE formulations for both PEC, and penetrable (plasmonic) and core-shell scatterers as well as introduce corresponding *characteristic mode* (CM) formulations. We'll also introduce a new CM formulation for core-shell structures. However, we start this chapter by introducing *the theory of characteristic modes* (TCM) and give motivation for its use, as sometimes the inverse of a scattering problem is to be solved: instead of looking for an unknown response of a known scatterer, a known response is sought for an unknown scatterer. Due to reciprocity one might assume this to be trivial, but as the coupling of a scatterer to an excitation behaves in a dot-product like sense, the true potential of a scatterer can not be studied by illuminating it with a simple excitation, but would instead require quasi-infinite excitations in quasi-infinite orientations.

TCM avoids this problem by studying excitation-independent eigencurrents, *modes*, that are able exist on a scatterer. Examples of eigencurrents are shown in Figure 4. *Resonating modes* are then those, whose reactive parts are zero, corresponding to the condition of *zero stored reactive energy*. As resonant modes are unable to store energy, must they dissipate it otherwise, i.e., as EM radiation (or heat) and thus the resonant modes correspond to power transmission, i.e., radiation maxima.

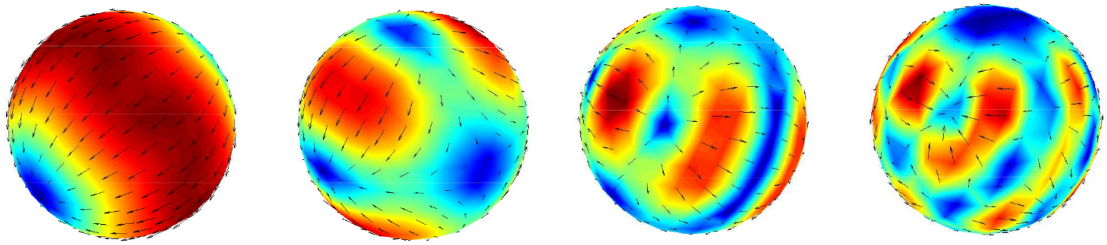

Figure 4: Eigencurrent solutions, modes, for a silver sphere (from left to right) for dipole, quadrupole, hexapole, and octopole

To illustrate TCM, consider a symmetric operator $\mathbf{Z}$, that behaves like an impedance operator, such, that it is able to map electric currents to electric fields. If the operator is $\mathbf{Z} = \mathbf{R} + i\mathbf{X}$, it can be decomposed in to its real and imaginary parts, $\mathbf{R}$ and $\mathbf{X}$, correspondingly. Characteristic modes for such system can be found from the following eigenvalue equation

$$\mathbf{X}(\mathbf{J}_n) = \lambda_n \mathbf{R}(\mathbf{J}_n) \tag{16}$$

where $\mathbf{J}_n$ is the nth eigenfunction, i.e., eigencurrent and λ_n the corresponding eigenvalue. As $\mathbf{X}$ and $\mathbf{R}$ are real and symmetric operators, must all eigenvalues and -vectors be real as well. [6] The eigenfunctions must also be *orthogonal*: no mode can be represented as a sum of other modes, i.e., *the projection of each mode to another should be zero*.

Found eigen-currents can then be used to expand a solution for a scattering problem through a *modal expansion*, i.e., the currents in the already introduced SEP

are found from

$$\mathbf{J} = \sum_n a_n \mathbf{J}_n \tag{17a}$$

$$\mathbf{M} = \sum_n b_n \mathbf{M}_n \tag{17b}$$

$$\tag{17c}$$

where the *modal expansion coefficients*, a_n and b_n, are found by normalizing the modes to unit power, resulting in

$$a_n = \frac{V_n}{1 + i\lambda_n} \tag{18}$$

where $V_n =< \mathbf{J}_n, \mathbf{F}^{inc} >$ is the *modal excitation coefficient* and $\mathbf{F}^{inc}$ contains the incident terms with their formulation dependent coefficients. [7] The magnetic expansion coefficients can then be found from the formulation dependent correlation between electric and magnetic currents. This can and sometimes should be formulated for the magnetic coefficients first, as on the dual of PEC, i.e., PMC, *perfect magnetic conductor*, the electric coefficients go to zero.

Even though analytical solutions for modal analysis and scattering problems exist, they're limited to simple shapes and geometries in simple materials, whereas numerical methods allow the prediction of arbitrary shapes in arbitrary materials as long as a computationally evaluable Green's function exists for them. Thus next we'll introduce *integral equation formulations* for both scattering and modal analysis, upon which computationally evaluable schemes can be built.

When case specific boundary conditions are applied to the Equations in (11), the unknowns might become *attached* and the solution of the system *uniquely defined*. Thus in the following chapter the most common *surface integral equations, (SIEs)* for different, well known scattering and modal problems are introduced and a new one for *core-shell structures* is formulated.

If the unknown currents in (9) are expressed as a superposition of one *caused* by primary sources, $\mathbf{J}^p$ and $\mathbf{M}^p$, and the one that *causes* the secondary sources, $\mathbf{J}^s$ and $\mathbf{M}^s$, the Equations (9) comes, noting that $\mathbf{n}_0 = -\mathbf{n}_1$

$$\begin{aligned}
\mathbf{J}_0 &= \mathbf{n}_0 \times \mathbf{H}_0 &&= \mathbf{J}_0^p + \mathbf{J}_0^s && (19a)\\
\mathbf{M}_0 &= -\mathbf{n}_0 \times \mathbf{E}_0 &&= \mathbf{M}_0^p + \mathbf{M}_0^s && (19b)\\
\mathbf{J}_1 &= \mathbf{n}_1 \times \mathbf{H}_1 &&= \mathbf{J}_1^s && (19c)\\
\mathbf{M}_1 &= -\mathbf{n}_1 \times \mathbf{E}_1 &&= \mathbf{M}_1^s && (19d)
\end{aligned}$$

Then if we device interface conditions so that the general boundary conditions, i.e., the continuity of the tangential components are fulfilled

$$(\mathbf{E}_0)_{tan} = (\mathbf{E}_1)_{tan} \implies \mathbf{M}_0 = -\mathbf{M}_1 \tag{20a}$$

$$(\mathbf{H}_0)_{tan} = (\mathbf{H}_1)_{tan} \implies \mathbf{J}_0 = -\mathbf{J}_1 \tag{20b}$$

and also introduce two *trace operators*, tangential, γ_t, and rotated tangential, γ_r, as

$$\gamma_t \mathbf{F} = -\mathbf{n} \times \mathbf{n} \times \mathbf{F}|_S \tag{21a}$$
$$\gamma_r \mathbf{F} = \mathbf{n} \times \mathbf{F}|_S, \tag{21b}$$

we then have the tools required for formulating SIEs for scattering problems. We'll begin with the simplest case, PEC, advancing then through characteristic modes with increasing complexity towards the the formulation for core-shell structures.

3.1 Perfect electric conductors

SIE formulations were first formulated for PEC structures for both scattering and TCM problems. This was due to their straightforwardness and utility, as the vast majority of traditional antennas can be approximated to be good conductors in their operational frequencies. However, as vast majority of classical antennas have rather simple or even analytical solutions, like mono- or dipoles, horn antennas etc., TCM was in slumber for quite some time after its discovery. Only the recent advancements in antenna *multiple-input-multiple-output* (MIMO) applications, especially mobile ones due to their low space and thus high mutual coupling, have sparked new interest in TCM due to its ability to effectively minimize mutual coupling systematically, without pseudo-random and thus slow, iterative processes. [8, 9]

As stated in Equation (2.2), on a boundary of a PEC the tangential component of an electric field must vanish. Thus when forming the surface equivalence, in which the magnetic current $\mathbf{M}$ is linearly dependent on $\mathbf{E}_{tan}$, must it vanish as well. As there is no field in domain Ω_1, there is no need for representation there, as illustrated in Figure 5. The Equations in (11) become for domain Ω_0, taking $\mathbf{n}_0 = -\mathbf{n}_1$

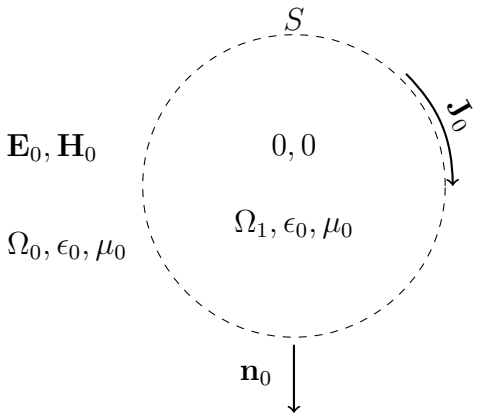

Figure 5: Surface equivalence representation of the scattering problem for a PEC scatterer in domain Ω_0, as the field inside Ω_1 vanishes.

$$\chi_0 \mathbf{E}_0 = \eta_0 \mathcal{T}_0[\mathbf{J}_S] + \mathbf{E}^p \tag{22a}$$
$$\chi_0 \mathbf{H}_0 = \mathcal{K}_0[\mathbf{J}_S] + \mathbf{H}^p. \tag{22b}$$

Then we push the field point to the surface S, where the scattered field is to perfectly nullify the original field to fulfil the PEC condition, i.e zero field inside, $\mathbf{E}_{tan} = 0$. However the tangential component of the magnetic field is not zero on the surface, and we must use the identities shown in the Equations (19a) and (10), i.e., replace $\gamma_t \mathbf{H}_0$ with $\mathbf{n} \times \mathbf{J}_0$ and χ with $\frac{1}{2}$, resulting in

$$-\gamma_t \mathbf{E}^p = \gamma_t \eta_0 \mathcal{T}_0[\mathbf{J}_S] \tag{23a}$$
$$-\gamma_r \mathbf{H}^p = \Big(\gamma_r \mathcal{K}_0 - \frac{1}{2}\mathbf{I}\Big)[\mathbf{J}_S] \tag{23b}$$

where I stands for the identity operator. These equations are known as *eletric field integral equation (EFIE)* and *magnetic field integral equation (MFIE)* respectively.

Both of these do have the tendency of suffering from non-physical *internal resonances*, that arise from the cavity resonator formed by the closed surface of the scatterer and thus *combined field integral equation (CFIE)* is often used instead, defined as

$$\frac{1}{\eta} EFIE + MFIE, \tag{24}$$

which is free of internal resonances and thus able to obtain valid results. [10]

For PEC scatterers, the TCM formulation arises naturally: if the sources in Equation (23) are supressed, one obtains

$$\gamma_t \eta_0 \mathcal{T}_0[\mathbf{J}_S] = 0 \tag{25a}$$
$$\Big(\gamma_r \mathcal{K}_0 - \frac{1}{2}\mathbf{I}\Big)[\mathbf{J}_S] = 0 \tag{25b}$$

which can be recognized to be of the same form as Equation (16), as it only contains terms operating on electric currents. However the eigenvalue equation has to be formed differently for them, one of them maps electric currents to electric field, $\mathbf{J}$ to $\mathbf{E}$, and the other currents to magnetic field, $\mathbf{J}$ to $\mathbf{H}$. As shown Dai et al. in [11], the eigenvalue equation for EFIE is exactly like the one represented in Equation (16), but the one for MFIE becomes

$$\mathbf{R}(\mathbf{J}_n) = -\lambda_n \mathbf{X}(\mathbf{J}_n). \tag{26}$$

In short, this arises due from our time harmonic formulation: as $\mathbf{H}$ is expressed through the curl of $\mathbf{E}$, which has the imaginary unit $-i$ etc., in its exponent, will the roles of $\mathbf{R}$ and $\mathbf{X}$ switch places.

As we will further discuss in Chapter 5, these both have the same problem as the scattering formulations, i.e., some of the obtained results are nonphysical, but they also have a similar remedy: as the spurious resonances are different in nature, CFIE CM analysis is able to produce spurious free solutions, corresponding to the actual, physical modes. CFIE CM is obtained similarly to scattering problems as a weighted linear combination of the EFIE and MFIE, however yet again resulting in a different eigenvalue equation

$$\Big(\mathbf{Z}_E + (1-\alpha)\eta_j \mathbf{Z}_H\Big)\mathbf{J}_n = (1+i\lambda_n)\Big(\alpha \mathbf{R}_E + (1-\alpha) i\eta_j \mathbf{X}_H\Big)\mathbf{J}_n \tag{27}$$

where the sub-indices of $\mathbf{E}$ and $\mathbf{H}$ refer to either EFIE or MFIE operator correspondingly and α is the weighting factor, often equal, i.e., 0.5, of the two formulations. [11]

3.2 Penetrable objects

With advanced manufacturing techniques and applications, scatterers were able to evolve as well - since the 1970s for instance microstrip antennas have included dielectrics. This is, as they are able to condense fields, thus diminishing the spatial requirements of antennas: if the wave can be condensed n-fold, so will the antenna, as it is linearly dependent on the wavelength. This is important, as shown by Harrington and Chu (and hence known as *Chu–Harrington limit*) already in the mid 20th century, the electrical size, i.e., the size of an antenna in wavelengths has a great effect on its dominant features. [12] In recent years the interest in plasmonics has also increased due to advancements in nanofabrification methods, and they can be modelled classically as penetrable objects as well via the already introduced Drude model. [13]

One of the earliest, most robust, physical and thus the most popular way to formulate the surface integral equation for penetrable objects is to use the *PMCHWT formulation* [14]. This can be obtained by taking directly the problem shown in Figure 3, i.e., Equation (11)., and then yet again enforcing the continuity of the tangential components on the surface S, resulting in

$$-\gamma_t \mathbf{E}^p = \gamma_t \sum_{j=0}^{1} \Big(\eta_j \mathcal{T}_j[\mathbf{J}_S] - \mathcal{K}_j[\mathbf{M}_S]\Big) \tag{28a}$$

$$-\gamma_t \mathbf{H}^p = \gamma_t \sum_{j=0}^{1} \Big(\mathcal{K}_j[\mathbf{J}_S] + \frac{1}{\eta_j}\mathcal{T}_j[\mathbf{M}_S]\Big). \tag{28b}$$

This can be then written in matrix equation form as

$$\gamma_t \begin{bmatrix} \eta_0\mathcal{T}_0 + \eta_1\mathcal{T}_1 & -(\mathcal{K}_0 + \mathcal{K}_1) \\ \mathcal{K}_0 + \mathcal{K}_1 & \frac{1}{\eta_0}\mathcal{T}_0 + \frac{1}{\eta_1}\mathcal{T}_1 \end{bmatrix} \begin{bmatrix} \mathbf{J}_S \\ \mathbf{M}_S \end{bmatrix} = -\gamma_t \begin{bmatrix} \mathbf{E}_0^p \\ \mathbf{H}_0^p \end{bmatrix} \tag{29}$$

where one can find familiar terms from the EFIE and MFIE formulations, of which the PMCHWT is combined of and is, similar to CFIE in PEC studies, free of spurious responses.

However modal analysis cannot be built upon PMCHWT formulation, as it cannot be decomposed properly into $\mathbf{X}$ and $\mathbf{R}$, having both magnetic and electric currents and for now *the existence of truly spurious free formulations is still open.* [15] There still are a few approaches, which are able to obtain reasonable results with similar computational effort, especially for plasmonics. One of these is based on splitting the equivalent magnetic current on the inner and outer surface, as shown in Figure 6. [16]

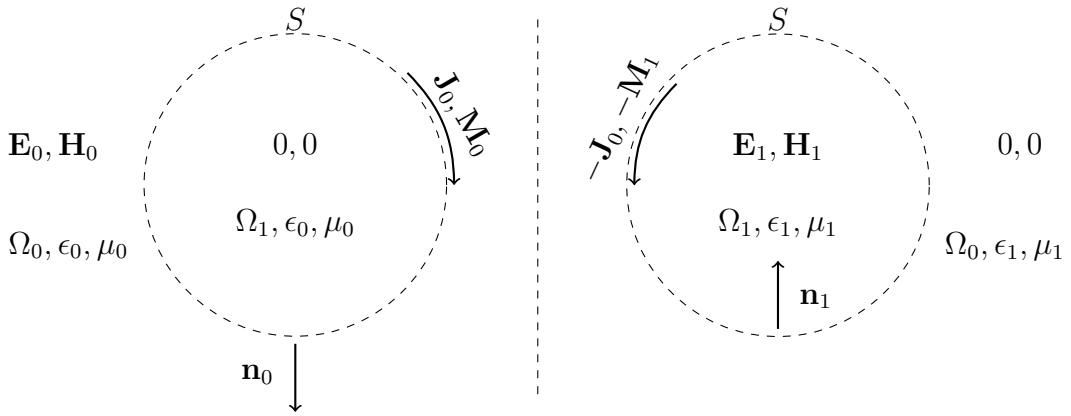

Figure 6: Surface equivalence representation of a modal problem of a penetrable scatterer for domain Ω_0 (left) and domain Ω_1 (right).

The field representations for the domains then become, taking $\mathbf{n}_1 = -\mathbf{n}_0$

$$\chi_0 \mathbf{E}_0 = \eta_0 \mathcal{T}_0[\mathbf{J}_0] - \mathcal{K}_0[\mathbf{M}_0] + \mathbf{E}^p \tag{30a}$$
$$-\chi_1 \mathbf{E}_1 = \eta_1 \mathcal{T}_1[\mathbf{J}_0] - \mathcal{K}_1[\mathbf{M}_1] \tag{30b}$$
$$\chi_0 \mathbf{H}_0 = \frac{1}{\eta_0} \mathcal{T}_0[\mathbf{M}_0] + K_0[\mathbf{J}_0] + \mathbf{H}^p \tag{30c}$$
$$-\chi_1 \mathbf{H}_1 = \frac{1}{\eta_1} \mathcal{T}_1[\mathbf{M}_1] + K_1[\mathbf{J}_0]. \tag{30d}$$

One of the magnetic currents can be expressed through the electric one if the Equation (30c) is pushed to the surface S:

$$\gamma_t \chi_0 \mathbf{H}_0 = \gamma_t \Big(\frac{1}{\eta_0} \mathcal{T}_0[\mathbf{M}_0] + \mathcal{K}_0[\mathbf{J}_0] + \mathbf{H}^p \Big) \tag{31}$$

replacing $\gamma_t \mathbf{H}_0$ again with $\mathbf{n} \times \mathbf{J}_0$

$$\frac{1}{\eta_0} \gamma_t \mathcal{T}_0[\mathbf{M}_0] = \gamma_t \Big(-\mathcal{K}_0[\mathbf{J}_0] - \frac{1}{2} \mathbf{n} \times \mathbf{J}_0 - \mathbf{H}^p \Big) \tag{32}$$

and finally, using notation $\mathcal{K}_{j,\pm}[\mathbf{F}] = (\mathcal{K}_j \pm \frac{1}{2} \mathbf{n} \times)[\mathbf{F}]$:

$$\mathbf{M}_0 = -\eta_0 (\gamma_t \mathcal{T}_0)^{-1} (\mathcal{K}_{0,+}[\gamma_t \mathbf{J}_0] + \gamma_t \mathbf{H}^p). \tag{33}$$

The second current can then be found from Equation (30d) in a similar manner, resulting in

$$\mathbf{M}_1 = -\eta_1(\gamma_t\mathcal{T}_1)^{-1}(\mathcal{K}_{1,-}[\mathbf{J}_0]). \tag{34}$$

Inserting (33) and (34) back into Equations (30a) and (30b) and the tangential components on the surface S results to

$$\gamma_t\mathbf{E}_0 = \eta_0\Big((\gamma_t\mathcal{T}_0 + \gamma_t\mathcal{K}_{0,-}(\gamma_t\mathcal{T}_0)^{-1}\gamma_t\mathcal{K}_{0,+})[\mathbf{J}_0] + (\gamma_t\mathcal{T}_0)^{-1}\gamma_t\mathcal{K}_0\mathbf{H}^p\Big) + \gamma_t\mathbf{E}^p \tag{35a}$$

$$-\gamma_t\mathbf{E}_1 = \eta_1\Big(\gamma_t\mathcal{T}_1 + \gamma_t\mathcal{K}_{1,+}(\gamma_t\mathcal{T}_1)^{-1}\gamma_t\mathcal{K}_{1,-}\Big)[\mathbf{J}_0]. \tag{35b}$$

After enforcing the continuity of the tangential components one obtains

$$\begin{aligned}\Big(\eta_0(\gamma_t\mathcal{T}_0 + \gamma_t\mathcal{K}_{0,-}(\gamma_t\mathcal{T}_0)^{-1})\gamma_t\mathcal{K}_{0,+} + \eta_1(\gamma_t\mathcal{T}_1 + \gamma_t\mathcal{K}_{1,+}(\gamma_t\mathcal{T}_1)^{-1}\mathcal{K}_{1,-})\Big)[\mathbf{J}_0] = \\ -\gamma_t(\mathcal{K}_{0,-}\mathcal{T}_0^{-1}\mathbf{H}^p + \mathbf{E}^p)\end{aligned} \tag{36}$$

which can be recognized as a (16) like equation after neglecting the primary fields. It is worth noting, that the equation holds a pattern: the only difference between the domain dependent terms is the subindex $\pm$. This is rather natural, as it related to the surface normal, which is complementary for the two domains, i.e., it seems, that the term follows the direction of the surface normal.

3.3 Core-shell structures

Even though the formulation of penetrable objects allows the simulation of arbitrary number of parallel materials, it does not allow for embedded or layered materials, i.e., *composite* or *core-shell structures*. As recent advancements in nanofabrification techniques has allowed the creation of novel structures, a need for formulations that are able to accurately foresee and engineer their properties has arisen as well. As the analytical solutions are limited to simple geometries, the need for an excitation independent, numerical, i.e., modal formulation can easily be justified.

As seen from Figure 7, the problem might seem quite intimidating at first. However with a concise, domain by domain implementation of SEP a formulation for both scattering and characteristic modes can be found. Due to added complexity we introduce an additional superscript to our notation, which is used to define on which surface an operator or variable is defined: for instance $\mathbf{J}_1^1$ is the current on surface S^1 on the side of domain Ω_1 whereas $\mathbf{J}_2^1$ is the current on surface S^1 on the side of domain Ω_2. This'll become important, as we reach the TCM formulation for core-shell structures.

Applying SEP to domain Ω_0 results to the familiar set up of Figure 6. This is also true for domain Ω_2: even though they are not defined on the same, both domains

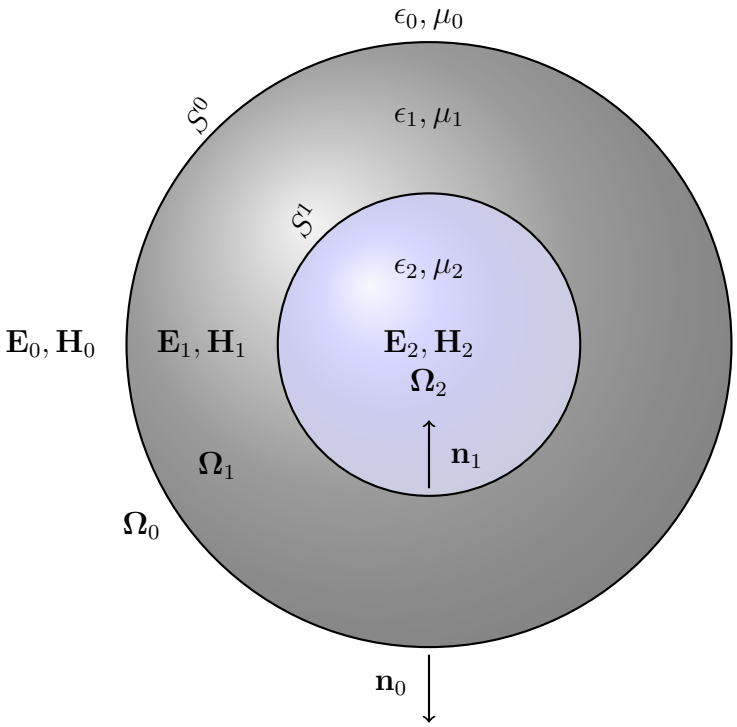

Figure 7: 2D-cut of a core-shell scattering problem.

are still *bounded only by one surface*, and thus we can directly write, only modifying in proper subscripts

$$\chi_j \mathbf{E}_j = \eta_j \mathcal{T}_j[\mathbf{J}_j] - \mathcal{K}_j[\mathbf{M}_j] + \delta_{j0}\mathbf{E}^p \tag{37a}$$

$$\chi_j \mathbf{H}_j = \frac{1}{\eta_j}\mathcal{T}_j[\mathbf{M}_j] + \mathcal{K}_j[\mathbf{J}_j] + \delta_{j0}\mathbf{H}^p \tag{37b}$$

$$j \in [0, 2].$$

However this isn't true to domain Ω_1, as it is encased by both surfaces 0 and 1, resulting to the following surface equivalence representation illustrated in Figure 8. From there the following equations are obtained naturally as a superposition of the fields caused by the currents on both surfaces as

$$\chi_1 \mathbf{E}_1 = -\sum_{j=0}^{1} \left(\eta_1 \mathcal{T}_1[\mathbf{J}_1^j] - \mathcal{K}_1[\mathbf{M}_1^j]\right) \tag{38a}$$

$$\chi_1 \mathbf{H}_1 = -\sum_{j=0}^{1} \left(\frac{1}{\eta_1}\mathcal{T}_1[\mathbf{M}_1^j] + \mathcal{K}_1[\mathbf{J}_1^j]\right). \tag{38b}$$

where the minus sign arises from the surface normals, that are defined out of the domain in which the fields are represented. We use only one representation for the

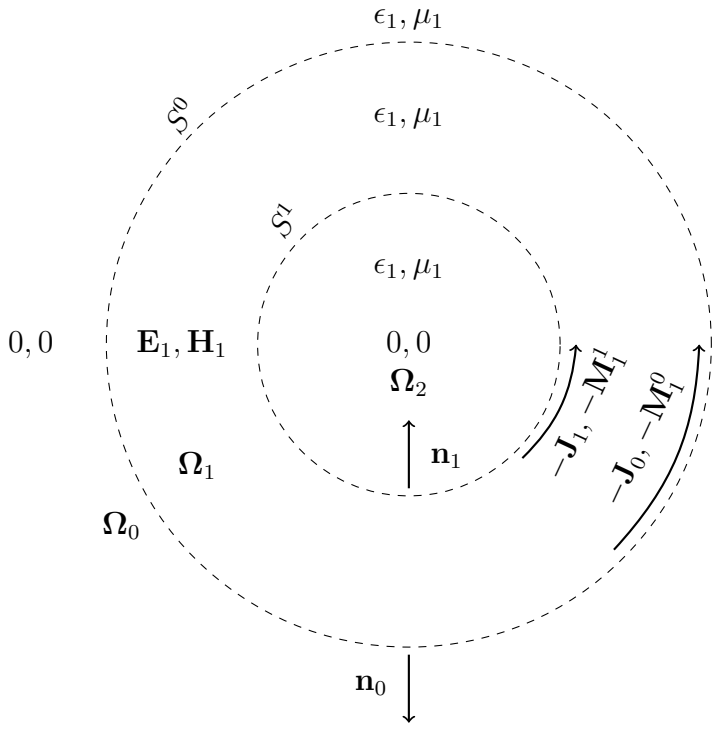

Figure 8: Surface equivalence representation for domain Ω_1 of the core-shell scattering problem.

electric current on a surface as in Equation (20a), i.e., $\mathbf{J}_0^0 + \mathbf{J}_1^0 = \mathbf{J}^0$, same holding for the magnetic current as well. To receive a proper system of equations, we then take the solution first to the surface S^0 and enforce the continuity of the tangential components over it, i.e., $\gamma_t \mathbf{E}_0 = \gamma_t \mathbf{E}_1$ and $\gamma_t \mathbf{H}_0 = \gamma_t \mathbf{H}_1$, resulting in

$$\gamma_t \Big(\sum_{j=0}^{1} \Big(\eta_j \mathcal{T}_j[\mathbf{J}^0] - \mathcal{K}_j[\mathbf{M}^0] \Big) + \eta_1 \mathcal{T}_1[\mathbf{J}^1] - \mathcal{K}_1[\mathbf{M}^1] \Big) = -\gamma_t \mathbf{E}^p \tag{39a}$$

$$\gamma_t \Big(\sum_{j=0}^{1} \Big(\mathcal{K}_j[\mathbf{J}^0] + \frac{1}{\eta_j} \mathcal{T}_j[\mathbf{M}^0] \Big) + \mathcal{K}_1[\mathbf{J}^1] + \frac{1}{\eta_1} \mathcal{T}_1[\mathbf{M}^1] \Big) = -\gamma_t \mathbf{H}^p. \tag{39b}$$

Then we do the same for surface S^1, enforcing the continuity of the tangential fields, $\gamma_t \mathbf{E}_1 = \gamma_t \mathbf{E}_2$ and $\gamma_t \mathbf{H}_1 = \gamma_t \mathbf{H}_2$

$$\gamma_t \Big(\eta_1 \mathcal{T}_1[\mathbf{J}^0] - \mathcal{K}_1[\mathbf{M}^0] + \sum_{j=1}^{2} \Big(\eta_j \mathcal{T}_j[\mathbf{J}^1] - \mathcal{K}_j[\mathbf{M}^1] \Big) \Big) = 0 \tag{40a}$$

$$\gamma_t \Big(\mathcal{K}_1[\mathbf{J}^0] + \frac{1}{\eta_1} \mathcal{T}_1[\mathbf{M}^0] + \sum_{j=1}^{2} \Big(\mathcal{K}_j[\mathbf{J}^1] + \frac{1}{\eta_j} \mathcal{T}_j[\mathbf{M}^1] \Big) \Big) = 0. \tag{40b}$$

and we have again the same number of equations and unknowns. These equations can be then written in matrix form as

$$\gamma_t \begin{bmatrix} \eta_0\mathcal{T}_0 + \eta_1\mathcal{T}_1 & -(\mathcal{K}_0 + \mathcal{K}_1) & \eta_1\mathcal{T}_1 & -\mathcal{K}_1 \\ \mathcal{K}_0 + \mathcal{K}_1 & \frac{1}{\eta_0}\mathcal{T}_0 + \frac{1}{\eta_1}\mathcal{T}_1 & \mathcal{K}_1 & \frac{1}{\eta_1}\mathcal{T}_1 \\ \eta_1\mathcal{T}_1 & -\mathcal{K}_1 & \eta_1\mathcal{T}_1 + \eta_2\mathcal{T}_2 & -(\mathcal{K}_1 + \mathcal{K}_2) \\ \mathcal{K}_1 & \frac{1}{\eta_1}\mathcal{T}_1 & \mathcal{K}_1 + \mathcal{K}_2 & \frac{1}{\eta_1}\mathcal{T}_1 + \frac{1}{\eta_2}\mathcal{T}_2 \end{bmatrix} \begin{bmatrix} \mathbf{J}^0 \\ \mathbf{M}^0 \\ \mathbf{J}^1 \\ \mathbf{M}^1 \end{bmatrix} = -\gamma_t \begin{bmatrix} \mathbf{E}^p \\ \mathbf{H}^p \\ 0 \\ 0 \end{bmatrix} \tag{41}$$

where one should recognize the resemblance to Equation (29): if split into two times two sub-matrices, the upper left and lower right terms have both currents and terms related to a single surface and are exactly identical to the PMCHWT formulation for a single layer scatterer, as is natural. The new terms, upper right and lower left however have terms that that give the fields on one surface due to currents on the other, and thus can be considered to be *cross-coupled terms*.

Obtaining the CM formulation for core-shell structures resembles the corresponding single layer penetrable scatterer formulation: instead of combining, the magnetic currents on each side of a surface are again kept separate. Then, as we yet again have too many variables for proper CM formulation, we express the magnetic currents as functions of the electric ones: if we solve for the magnetic current in domain Ω_0 on surface S^0, i.e., $\mathbf{M}_0^0$ from (37b) on the surface S^0 and thus replace $\gamma_t\mathbf{H}_0$ with $\mathbf{n}\times\mathbf{J}_0$, we obtain

$$\frac{1}{2}\mathbf{n}_0 \times \mathbf{J}_0 = \gamma_t\Big(\frac{1}{\eta_0}\mathcal{T}_0[\mathbf{M}_0^0] + \mathcal{K}_0[\mathbf{J}_0] + \mathbf{H}^p\Big) \tag{42}$$

reordering the terms and using the notation $\mathcal{K}_{j,\pm}[\mathbf{F}] = (\mathcal{K}_j \pm \frac{1}{2}\mathbf{n}\times)[\mathbf{F}]$ results to

$$\mathbf{M}_0^0 = -\eta_0(\gamma_t\mathcal{T}_0)^{-1}\Big(\mathcal{K}_{0,-}[\mathbf{J}_0] + \mathbf{H}^p\Big). \tag{43}$$

The magnetic current on the inner surface S^1, i.e., $\mathbf{M}_2^1$ is found in a similar manner, resulting in

$$\mathbf{M}_2^1 = -\eta_2(\gamma_t\mathcal{T}_2)^{-1}\Big(\mathcal{K}_{2,+}[\mathbf{J}_1]\Big). \tag{44}$$

However the magnetic currents in the domain bounded by two surfaces cannot be solved for in a similar manner due to the cross coupled terms. Instead, we assemble a system of equations by first taking Equation (38b) to both surfaces 0 and 1

$$\frac{1}{2}\mathbf{n}_0 \times \mathbf{J}_0 = -\gamma_t\Big(\frac{1}{\eta_1}\mathcal{T}_1([\mathbf{M}_1^0] + [\mathbf{M}_1^1]) + \mathcal{K}_1([\mathbf{J}_0] + [\mathbf{J}_1])\Big) \tag{45a}$$

$$\frac{1}{2}\mathbf{n}_1 \times \mathbf{J}_1 = -\gamma_t\Big(\frac{1}{\eta_1}\mathcal{T}_1([\mathbf{M}_1^0] + [\mathbf{M}_1^1]) + \mathcal{K}_1([\mathbf{J}_0] + [\mathbf{J}_1])\Big) \tag{45b}$$

which result, after reordering, to

$$\gamma_t\Big(\mathcal{K}_{1,+}[\mathbf{J}_0] + \mathcal{K}_1[\mathbf{J}_1]\Big) = -\gamma_t\Big(\frac{1}{\eta_1}\mathcal{T}_1([\mathbf{M}_1^0] + [\mathbf{M}_1^1])\Big) \tag{46a}$$

$$\gamma_t\Big(\mathcal{K}_1[\mathbf{J}_0] + \mathcal{K}_{1,+}[\mathbf{J}_1]\Big) = -\gamma_t\Big(\frac{1}{\eta_1}\mathcal{T}_1([\mathbf{M}_1^0] + [\mathbf{M}_1^1])\Big). \tag{46b}$$

If this is further written in matrix form:

$$\gamma_t \begin{bmatrix} \frac{1}{\eta_1}\mathcal{T}_1 & \frac{1}{\eta_1}\mathcal{T}_1 \\ \frac{1}{\eta_1}\mathcal{T}_1 & \frac{1}{\eta_1}\mathcal{T}_1 \end{bmatrix} \begin{bmatrix} \mathbf{M}_1^0 \\ \mathbf{M}_1^1 \end{bmatrix} = -\gamma_t \begin{bmatrix} \mathcal{K}_{1,+} & \mathcal{K}_1 \\ \mathcal{K}_1 & \mathcal{K}_{1,+} \end{bmatrix} \begin{bmatrix} \mathbf{J}_0 \\ \mathbf{J}_1 \end{bmatrix} \tag{47}$$

and denoting as follows

$$-\begin{bmatrix} \frac{1}{\eta_1}\gamma_t\mathcal{T}_1 & \frac{1}{\eta_1}\gamma_t\mathcal{T}_1 \\ \frac{1}{\eta_1}\gamma_t\mathcal{T}_1 & \frac{1}{\eta_1}\gamma_t\mathcal{T}_1 \end{bmatrix}^{-1} \gamma_t \begin{bmatrix} \mathcal{K}_{1,+} & \mathcal{K}_1 \\ \mathcal{K}_1 & \mathcal{K}_{1,+} \end{bmatrix} = \begin{bmatrix} A & C \\ B & D \end{bmatrix} \tag{48}$$

results in

$$\mathbf{M}_1^0 = A\mathbf{J}_0 + C\mathbf{J}_1 \tag{49a}$$
$$\mathbf{M}_1^1 = B\mathbf{J}_0 + D\mathbf{J}_1. \tag{49b}$$

Then we yet again follow the path similar to earlier formulations: if the magnetic currents in (43, 44), (49a) and (49b) are inserted to the electric field representations in (37a) and (38a) on corresponding surfaces, one obtains

$$\gamma_t\chi_0\mathbf{E}_0 = \eta_0\Big(\gamma_t\mathcal{T}_0 + \gamma_t\mathcal{K}_0(\gamma_t\mathcal{T}_0)^{-1}\gamma_t\mathcal{K}_{0,-}\Big)[\mathbf{J}_0] + \gamma_t\mathcal{K}_0\mathbf{H}^p + \gamma_t\mathbf{E}^p \tag{50a}$$
$$-\gamma_t\chi_1\mathbf{E}_1 = \gamma_t\Big((\eta_1\mathcal{T}_1 - \mathcal{K}_1(A+B))[\mathbf{J}_0] + (\eta_1\mathcal{T}_1 - \mathcal{K}_1(C+D))[\mathbf{J}_1]\Big) \tag{50b}$$
$$\gamma_t\chi_2\mathbf{E}_2 = \eta_2\Big(\gamma_t\mathcal{T}_2 + \gamma_t\mathcal{K}_2(\gamma_t\mathcal{T}_2)^{-1}\gamma_t\mathcal{K}_{2,-}\Big)[\mathbf{J}_1]. \tag{50c}$$

Here one should recognize the familiarity with Equation (35a), the only difference yet again lying in the domain bounded by two surfaces. As we have two unknowns, the currents on surfaces 0 and 1, we reduce our number of equations by enforcing the continuity of the tangential components, without the primary fields, resulting in

$$\begin{aligned} 0 = \Big(&\Big(\eta_0(\gamma_t\mathcal{T}_0 + \gamma_t\mathcal{K}_0(\gamma_t\mathcal{T}_0)^{-1}\gamma_t\mathcal{K}_{0,-}) + \eta_1\gamma_t\mathcal{T}_1 - \gamma_t\mathcal{K}_1(A+B)\Big)[\mathbf{J}_0] + \\ &\Big(\eta_1\mathcal{T}_1 - \mathcal{K}_1(C+D)\Big)[\mathbf{J}_1]\Big), \\ &\mathbf{r} \in S^0 \end{aligned} \tag{51a}$$

$$\begin{aligned} 0 = \Big(&\Big((\eta_1\gamma_t\mathcal{T}_1 - \gamma_t\mathcal{K}_1(A+B))\Big)[\mathbf{J}_0] + \\ &\Big((\eta_1\gamma_t\mathcal{T}_1 - \gamma_t\mathcal{K}_1(C+D) + (\eta_2\gamma_t\mathcal{T}_2 + \gamma_t\mathcal{K}_2(\gamma_t\mathcal{T}_2^{-1}\gamma_t\mathcal{K}_{2,-})\Big)[\mathbf{J}_1]\Big), \\ &\mathbf{r} \in S^1 \end{aligned} \tag{51b}$$

which then can be written again in matrix form as

$$\begin{bmatrix} Z_{11} & Z_{12} \\ Z_{21} & Z_{22} \end{bmatrix} \begin{bmatrix} \mathbf{J}_0 \\ \mathbf{J}_1 \end{bmatrix} = \begin{bmatrix} 0 \end{bmatrix}, \tag{52}$$

where the submatrices are now as follows

$$Z_{11} = \eta_0(\gamma_t\mathcal{T}_0 + \gamma_t\mathcal{K}_0(\gamma_t\mathcal{T}_0)^{-1}\gamma_t\mathcal{K}_{0,-}) + \eta_1\gamma_t\mathcal{T}_1 - \gamma_t\mathcal{K}_1(A+B) \tag{53a}$$
$$Z_{12} = \eta_1\gamma_t\mathcal{T}_1 - \gamma_t\mathcal{K}_1(C+D) \tag{53b}$$
$$Z_{21} = \eta_1\gamma_t\mathcal{T}_1 - \gamma_t\mathcal{K}_1(A+B) \tag{53c}$$
$$Z_{22} = \eta_1\gamma_t\mathcal{T}_1 - \gamma_t\mathcal{K}_1(C+D) + \eta_2(\gamma_t\mathcal{T}_2 + \gamma_t\mathcal{K}_2(\gamma_t\mathcal{T}_2)^{-1}\gamma_t\mathcal{K}_{2,-}). \tag{53d}$$

Here one should yet again note the symmetry of the solution, which is again quite natural.

Even though formulated here through two magnetic currents, multiple other possible combinations exist for the creation of the TCM formulation for core-shell structures, all exhibiting slightly different behaviour. As their derivation is exactly similar, step by step, and thus straightforward, they aren't introduced here. Also worth noting is that the introduced formulation can be extended easily for n-layered structures, as they all can be decomposed into domains that are bounded either by a single or two surfaces, and thus they follow exactly the same pattern as introduced here. This is guaranteed by the trick in the direction of the surface normals, following the rule

$$\text{sign}(\mathbf{n}_j) = -1^j \tag{54}$$

where j is the surface on which the normal is to be defined. The introduced procedure is also valid for arbitrary number of parallel surfaces, i.e., surfaces that are embedded into a domain already bounded by a surface, as shown in Figure 9.

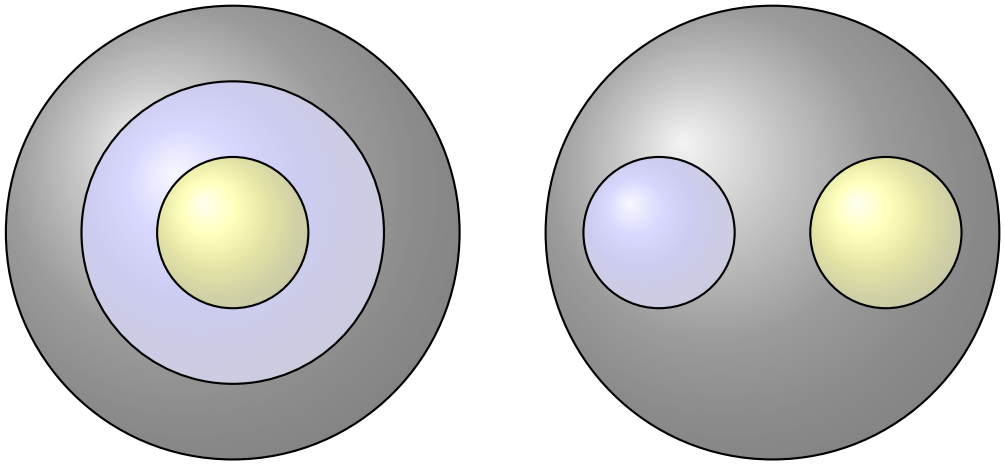

Figure 9: Examples of problems, for which the formulation generalizes systematically. Different colors depict material domains, which can be any arbitrary material, as long as they can be evaluated with a SIE formulation properly.

We now have at our disposal a family of SIEs for scattering and modal analysis. In the following chapter we'll develop numerical schemes, with which general EM

problems can be attacked with - it is important to note, that so far all we've introduced holds true in exact sense, as we're only representing the original problem through an equivalent problem. The solution becomes approximate as we *discretize* our computational domain and start to seek for a solution in a *weighted average sense*. However this is the price to be paid if complex structures are to be analyzed, for which no analytical solution can be devised.

4 Numerical solutions

Even though discussed, so far we've not introduced anything computationally evaluable as such. In this chapter we'll introduce a background needed for the numerical solution of the equations, starting with weak formulation and then going through testing to how the desired quantities are finally calculated.

4.1 Weak formulation

As our governing integral equations have both divergence and gradient operating, the solution is not trivial to find: the gradient requires continuity and the divergence normal continuity of the unknown. Also, as the Green's function in the operator S is singular and thus hardly integrable, its derivative is even more singular. Even though some techniques exist that help the evaluation of the Greens function, like singularity subtraction technique [17], generally the solution to our equation can not be found easily in the strong sense.

However with the help of *weak formulation* we can transfer one of the ∇ operators to a *test function*. For EFIE the weak formulation is obtained by taking Equation (23a), using the definition of the operator $\mathcal{T}$, multiplying with a suitable test function $\mathbf{v}$, that can be defined as a vector field tangential to the surface S, automatically taking the tangential component. Then integrating over domain Ω results in

$$-\left\langle \mathbf{v}, \mathbf{E}^p \right\rangle_S = \eta_0 \frac{-1}{ik_0} \left\langle \mathbf{v}, \nabla \mathcal{S}[\nabla_S \cdot \mathbf{J}_s] \right\rangle_S + ik_0 \left\langle \mathbf{v}, \mathcal{S}[\mathbf{J}_S] \right\rangle_S. \tag{55}$$

Then studying the solution on the surface S and applying the divergence product rule, i.e.,

$$u\nabla_S \cdot \mathbf{F} = -\nabla_S \cdot (u\mathbf{F}) + \nabla_S u \cdot \mathbf{F}, \tag{56}$$

on the first term on the RHS of Equation (55) results in

$$\left\langle \mathbf{v}, \nabla \mathcal{S}[\nabla_S \cdot \mathbf{J}_s] \right\rangle_{dS} = \left\langle \nabla_S \cdot \mathbf{v}, \mathcal{S}[\nabla_S \cdot \mathbf{J}_s] \right\rangle_{dS} - \left\langle \nabla_S, \mathbf{v}\mathcal{S}[\nabla_S \cdot \mathbf{J}_s] \right\rangle_{dS} \tag{57}$$

where the second term on the RHS should be recognized as the *Gauss's law*, making the term go to zero for a closed surface, applicable as long as $\nabla_s \cdot \mathbf{J}_s$ is well defined, i.e., $\mathbf{J}_s$ is normally continuous. After substituting this back into Equation (55) the following is obtained

$$\eta_0 \Big(\frac{1}{ik_0} \left\langle \nabla_S \cdot \mathbf{v}, \mathcal{S}[\nabla_S \cdot \mathbf{J}_s] \right\rangle_S + ik_0 \left\langle \mathbf{v}, \mathcal{S}[\mathbf{J}_S] \right\rangle_S \Big) = -\left\langle \mathbf{v}, \mathbf{E}^p \right\rangle_S \tag{58}$$

which is the weak form of EFIE. The weak formulations for the other IEs can be found in a similar manner but are not introduced here due to some details required in their formlation, which'd take away the focus from the emphasis of this work. For instance as MFIE is formulated through the rotated tangential components of the fields, using similar test functions as in EFIE will result into a weak form that doesn't properly test the boundary conditions of the original system, i.e., they're not fulfilled, even in *the weak*, i.e., weighted average sense.

Next we'll introduce how a linear system of equations is formed from the weak formulation.

4.2 Basis functions and testing

One should note, that in the previous section the conditions set for the unknown function $\mathbf{J}_s$ are relaxed, as one of the derivatives is transferred to the test function $\mathbf{v}$. However this means that our test function should be normally continuous like the unkown as well. This is an important property of weak formulations: they tell how the unknown should be tested for a proper solution to exist. For instance, as mentioned, the testing of EFIE and MFIE have to be done by different basis functions to ensure proper fulfilment of boundary conditions. [18] In conclusion one should always use such test functions $\mathbf{v}_n$ that fulfill the weak form of the formulation under evaluation.

If we expand the unknown, here the electric current, as a linear combination of known functions $\mathbf{u}_n$, known as *basis functions*

$$\mathbf{J}_s \approx \sum_{n=1}^{N} c_n \mathbf{u}_n \tag{59}$$

where c_n are the unknown coefficients of the N basis functions, approximating the real solution $\mathbf{J}_s$. If we insert the approximation back into the weak formulation and split the integration over the domain into a sum of integrals over the support S_n, where $\mathbf{u}_n$ is defined, we'll have a system of n linear equations. This means that our original problem of looking for an unknown vector function has been turned into a problem of looking for unknown scalar coefficients from a linear system of equations

$$\mathbf{Ax} = \mathbf{b} \tag{60}$$

where an element $\mathbf{A}_{nk}$ contains the integrals over the element S_n for test function $\mathbf{v}_n$ versus basis function $\mathbf{u}_k$, i.e.,

$$\mathbf{A}_{nk} = \frac{1}{ik_0}\Big\langle \nabla_S \cdot \mathbf{v}_n, \mathcal{S}[\nabla_S \cdot \mathbf{u}_k] \Big\rangle_{S_n} + ik_0 \Big\langle \mathbf{v}_n, \mathcal{S}[\mathbf{u}_k] \Big\rangle_{S_n}, \tag{61}$$

an element $\mathbf{b}_n$ contains the sources on that element

$$\mathbf{b}_n = -\Big\langle \mathbf{v}_n, \gamma_t \mathbf{E}^p \Big\rangle_{S_n} \tag{62}$$

and $\mathbf{x}_n$ the unknown coefficient c_n. Now our original problem of looking for an unknown function has been transferred to one of finding unknown scalar coefficients, which is widely referred to as *method of moments* (MoM). [19] From here the unknown scalar coefficients of the basis functions, c_n can easily be solved computationally, and multiple advanced algorithms exist solely for this purpose.

In the *Galerkin's method of weighted residuals*, the weak formulation must be tested with the basis functions, i.e., $\mathbf{v} = \mathbf{u}$. In the case of EFIE this is rather natural, as they both should satisfy the same criterion due to the weak formulation: normal continuity of the component tangential to the surface. A special case of

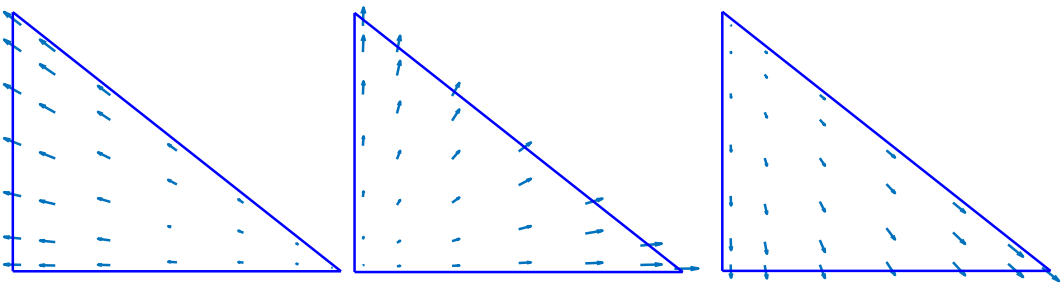

Figure 10: First order vector edge shape functions for a triangular element in reference coordinates

diverge conforming basis functions are the so called *Rao-Wilton-Glisson (RWG)* basis functions, shown in Figure 11, which are edge basis functions scaled by the length of the edge and surface area, i.e.,

$$\mathbf{v}_n = \begin{cases} \frac{l_n}{2A_n^+}(\mathbf{p}_n^+ - \mathbf{r}), \text{if } r \in \mathbf{T}_n^+ \\ -\frac{l_n}{2A_n^-}(\mathbf{p}_n^- - \mathbf{r}), \text{if } r \in \mathbf{T}_n^- \end{cases} \tag{63}$$

where $\mathbf{v}_n$ is the nth basis/test function, l_n the length of edge $\mathbf{e}_n$ associated with corresponding $\mathbf{v}_n$, $A_n^{\pm}$ the area of the corresponding element, and $\mathbf{p}_n^{\pm}$ a point in an element $\mathbf{T}_n^{+,-}$, where the sign is used to orientate the basis function properly [20]. RWG can be built by utilizingh first order vector edge shape functions, illustrated in Figure 10. The RWG basis functions are shown to provide good accuracy with EFIE and is widely used even for MFIE, even though it does not properly test the weak form of $\mathbf{n}\times$ formulations and thus might produce highly erroneous results for anything except the numerically easiest of test cases. If MFIE or other similar formulation is to be properly evaluated, the *Buffa-Christiansen* (BF) test functions should be used. [21]

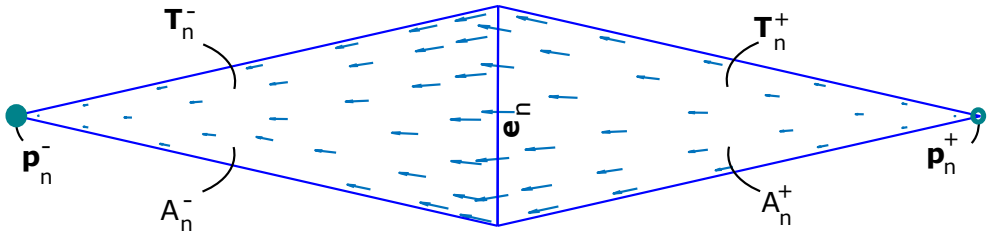

Figure 11: RWG basis function for triangular elements

Discretization is the point, at which our solution starts to diverge from the accurate one: if we increase the number of used basis functions, our approximate solution should converge towards the accurate solution, as long as our system of equations is *well-conditioned* and *stable*. Condition number is a figure of merit for a numerical method, that describes how much a small change in the input changes

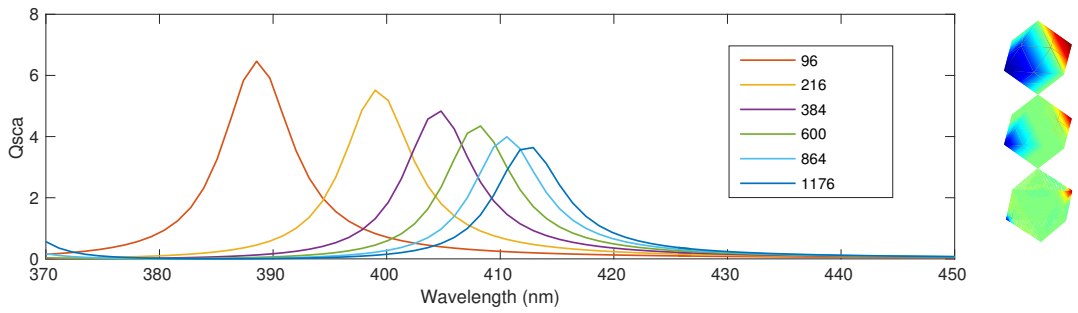

Figure 12: Converging solution of the Q_{sca} of a 50mm silver octahedron in the plasmonic regime for different degrees of freedom. On the right the surface charge distribution at the main peak is shown in the case of 96, 600 and 1176 degrees of freedom. Not introduced here, but the range of the colormaps change also drastically as the singular solutions at the sharp corners are approached.

the output. For matrices this generally describes the ratio between its smallest and biggest elements and determines the maximum available accuracy of the system, theoretically approaching zero as condition number approaches infinity.

An example of convergence is shown in Figure 12, where one should notice that as we're looking for a solution in a weighted average sense, low order discretization tends to smooth out and average the true solution, in the case of the octahedron resulting in greatly overestimated scattering peak as well as a blue shifted, i.e., higher in frequency shifted location. This can be understood with the basic principles from statics: strong gradients of surfaces, especially discontinuities of their normal vector, tend to have strong gradients of charge and thus field distributions and if we have large discretization elements and test point at the location of the natural singularity, the obtained result will be overestimated. If we were to study similar behaviour for an electrically small sphere, i.e., a smooth scatterer with a rather stable charge and/or current distribution, the solution would converge even with a small number of discretization elements, as shown in Figure 13. In this work all the introduced results are for smooth surfaces where the effect of discretization has been properly analyzed. Hence the quality of the discretization won't be further discussed in this work.

It is also important to note, that due to aliasing etc., it is possible to have converging behaviour towards a wrong solution as well, and thus one should always be careful when evaluating numerical solutions, as else one can easily receive a classical *garbage in,garbage out* -situation. It is worth mentioning, that this isn't only a problem of numerical formulations: almost all solutions, analytical or not, have sets of parameters that make them ill-defined or non-physical.

In modal analysis the discretization has another significant effect: a system of equations has always as many eigensolutions as it has degrees of freedom. This means, that the vast majority of modes for a too densely discretized have a minimalistic effect on the response of a scatterer and are thus a waste of computational resources, whereas a poorly discretized domain is not able to represent all of its physical modes.

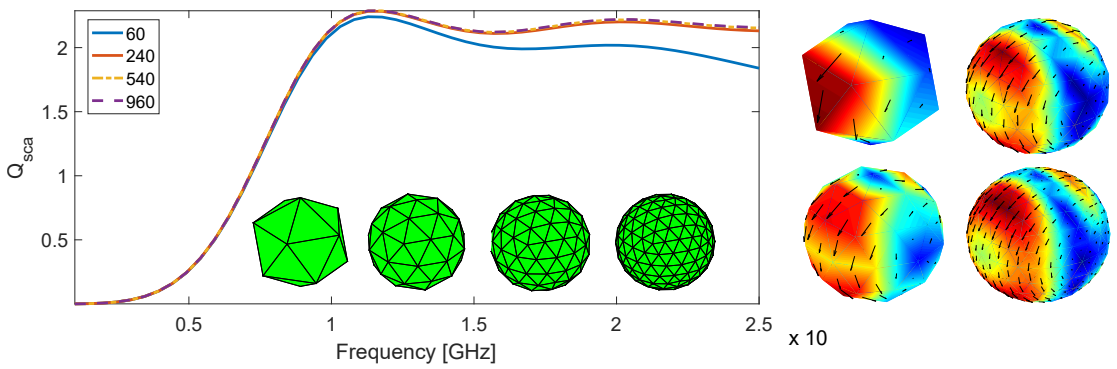

Figure 13: Converging solution of the Q_{sca} of a 10cm PEC sphere for different degrees of freedom. On the right the obtained equivalent electric current distribution is shown at 25 GHz.

Thus one should always use high discretization and postprosessing when performing modal analysis.

Now we have the method to compute numerical results for a wide range of EM problems. In the next section we'll introduce how the obtained results can be refined into well known figures of merit.

4.3 Extraction of results

For scattering problems, the system of equations formed (60) will return as a solution the vector $\mathbf{x}$. As they're only the coefficients for the basis functions, with them alone much analysis can't be done. However they do already give minor insight into the response at hand: the amount of extrema depicts the order of the mode active on the scatterer, and based upon their vectorial properties one can analyze if either magnetic or electric properties are dominating. This is, as diverging electric currents are related to equivalent electric charge and rotational to magnetic charge, i.e.,

$$\mathbf{n} \cdot \mathbf{D} = \frac{1}{i\omega} \nabla_S \cdot \mathbf{J} \quad \text{and} \quad \mathbf{n} \cdot \mathbf{B} = \frac{1}{iw} \nabla_S \times \mathbf{M} \tag{64}$$

examples of which are seen in Figure 14.

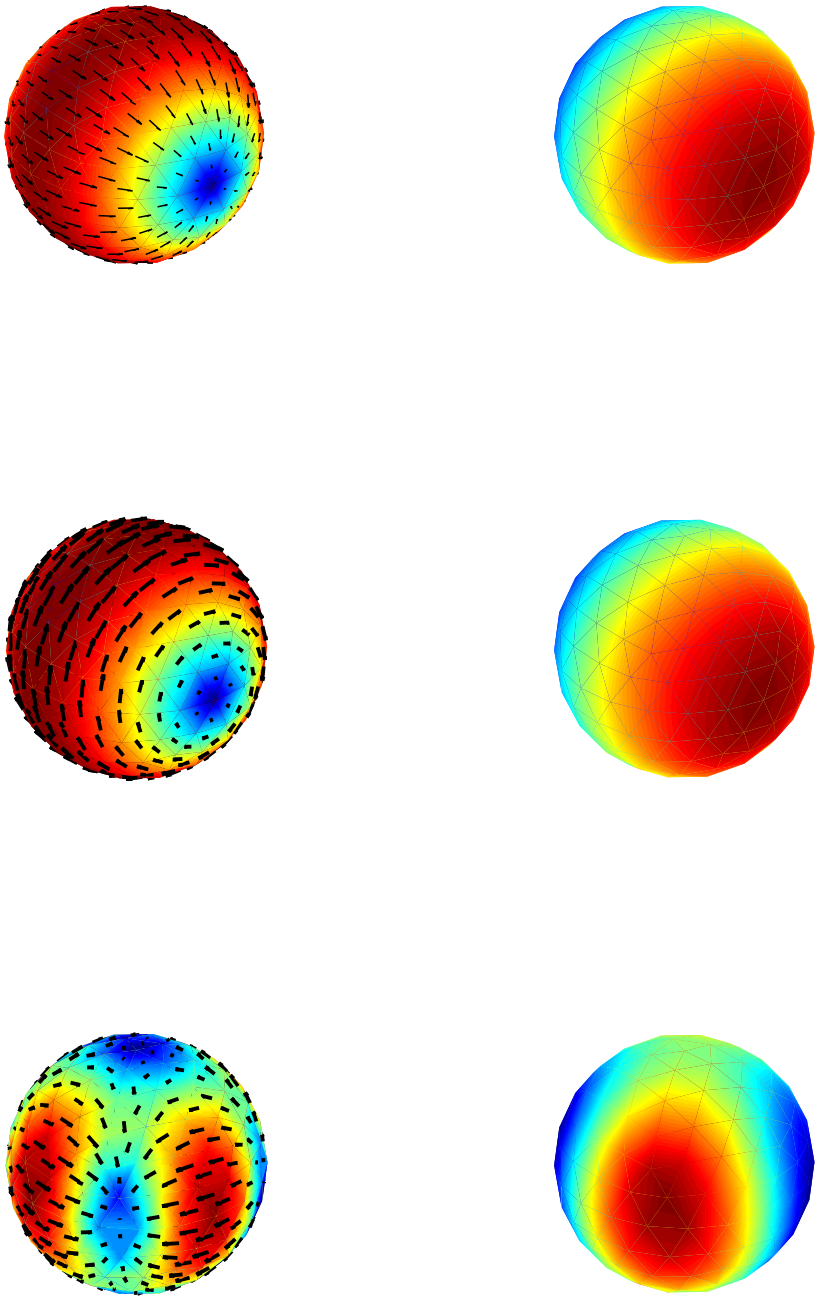

Figure 14: Relationship between currents and charge. On top row electric current has been plotted against electric charge: the diverging electric current results to an electric dipole. On the middle row electric current has been plotted against magnetic charge: rotational electric current leads to a magnetic dipole. On bottom row electric current has been plotted against electric charge: seemingly rotational current is actually diverging in nature and thus produces an electric multipole.

The scattering quantities can then be found from

$$P_{sca} = -\frac{1}{2}\mathfrak{Re}(\mathbf{x}^t \mathbf{A}_{ext}\mathbf{x}) \tag{65}$$

where the subscript of $\mathbf{A}_{ext}$ just denotes, that only the terms related to the outer surface, that produce fields to the outer domain should be used. [22] P_{abs} can then be easily found by subtracting the scattered power from the incident power.

In modal analysis solving the eigenvalue equation directly returns the coefficients of the eigen-currents, $\mathbf{J}_n$ and $\mathbf{M}_n$, as well as their eigenvalus λ_n. However if evolution of a mode is to be inspected over a frequency sweep, it is important to be able to automatically distinguish modes from another. Here the orthogonality properties of modes are of utmost importance: if one takes a projection of a mode at frequency j unto another at frequency $j+1$ and divides by the projection of the modes unto itself, i.e,

$$proj_{norm,nm} = \frac{\mathbf{J}_n^j \cdot \mathbf{J}_m^{j+1}}{\mathbf{J}_n^j \cdot \mathbf{J}_n^j} \tag{66}$$

one should receive something close to unity for the same mode and close to zero for other modes. This is tested for three random modes versus all other for a system with some 700 degrees of freedom in Figure 15

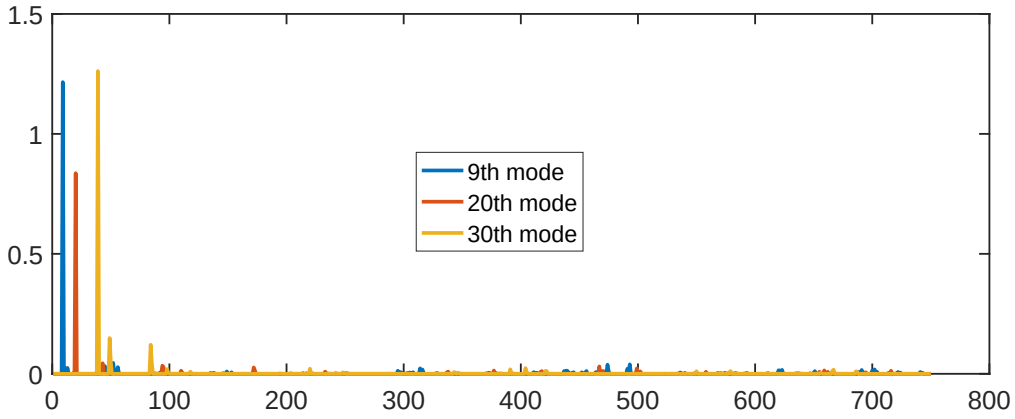

Figure 15: Normalized projections of modes against others for a PEC sphere at f $\approx 130MHz$.

where one can note that the projection of a mode on itself between near enough frequencies indeed seems to approach one and is more or less zero for the others. However under numerical tests during this work it was found out, that for strongly singular solutions the projections no longer always behave nicely, and thus, although slower, more robust algorithms based on not accepting the first value over a set criterion but maxima of the hole set were used instead.

5 Numerical results

In this section some results based on the introduced formulations are shown. All of the results are obtained with self-made MATLAB programs, which do however heavily rely upon earlier work of Aalto University School of Electrical Engineering Dpt. of Radio Science and Engineering [23, 24]. The meshing as well as the evaluation of integrals is done by the already implemented programs whereas self-implemented parts include the formulations, i.e., how the Equations (23b), (26), (27), (29), (36), (41) and (52) are organized and the received matrices turned to figures of merit, as shown in section 4.3.

The section PEC discusses the differences of CFIE, EFIE and MFIE via an example, in section plasmonics it is shown how modal solutions can be verified against an analytical solution and finally in the section core-shell the new CM formulation for multi-layered structures is verified.

5.1 Perfect electric conductors

Let's first replicate the results introduced in the [11], i.e., study the EM response and characteristic modes of a one meter radius sphere with EFIE, MFIE and CFIE based formulations. The received Q_{sca}, i.e., electrical size normalized scattering power is introduced in Figure 16. As one should note, the common consensus of MFIE solution failing dramatically for closed surfaces is well apparent in the results, that greatly underestimate the EM response of the scatterer under inspection. However the EFIE solution seems rather stable and thus the next natural step is to study the numerical stability, i.e., conditioning of the formulations.

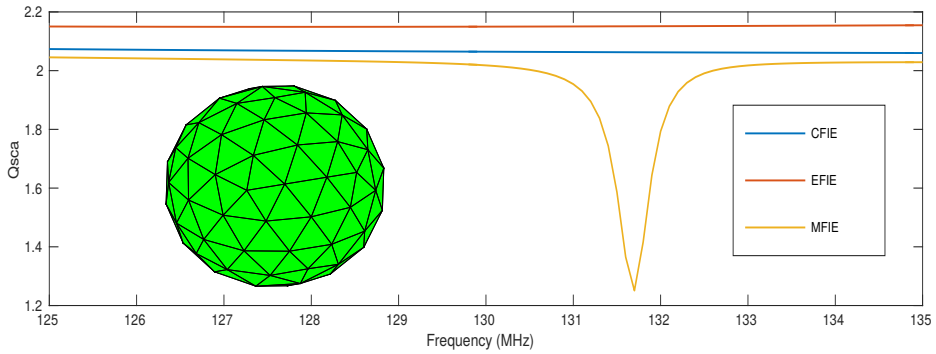

Figure 16: EM response of a 2 m diameter sphere as a function of frequency for EFIE, MFIE and CFIE

If one looks at the condition number introduced in Figure 17, one should note that the condition number for EFIE is many orders of magnitude lower than those of both EFIE and MFIE, MFIE of which seems to compete in its own league. This arises yet again from the different nature of the formulations, and a more suitable

a choice for comparison would've been M_{re}. As this tells us only how, no why the methods fail, the next step is to study the obtained equivalent current results of the formulations.

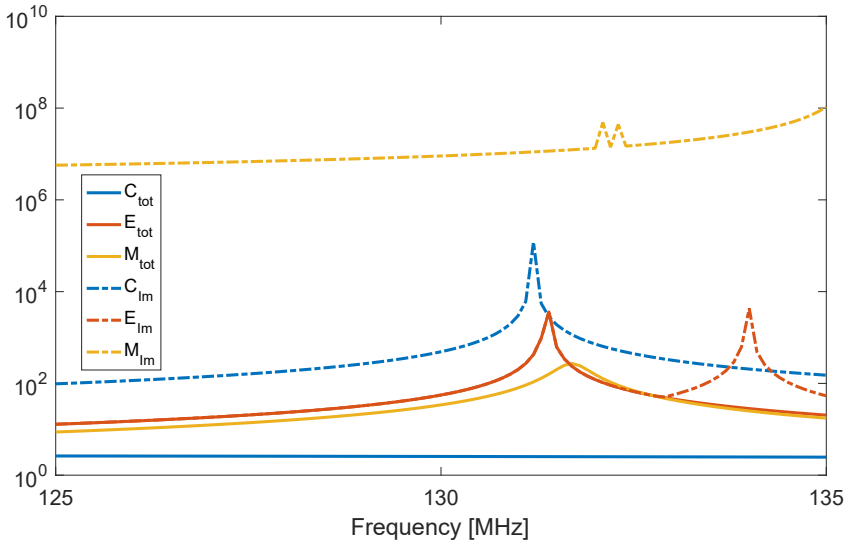

Figure 17: Condition numbers of the total $\mathbf{Z}$ matrices as well as their imaginary parts for the three formulations in the case of a 1 m radius PEC sphere.

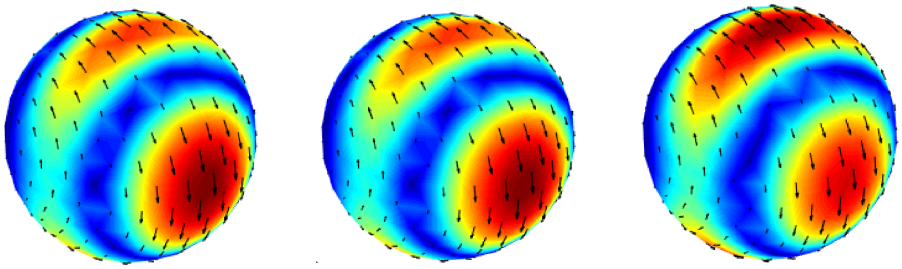

Figure 18: Current results (total) on the scatterer at the frequency of the internal resonance, $f \approx 131$ MHz, for (from left to right) CFIE, EFIE and MFIE

However the result obtained for the scattering problem introduced in Figure 18 doesn't shed much light on the reasons behind the failure: even though the scales are equal for all three plots, only MFIE solution seems to differ from the rest and only minorly. However, if one subtracts both EFIE and MFIE results from the CFIE results a, i.e., takes their difference, as is done in Figure 19 and uses it in unison with information from the Figure 20, it seems that EFIE fails for an electric mode (diverging currents) and MFIE for magnetic mode (rotational currents). This in

unison with the fact that EFIE and MFIE differ in formulation through the imaginary unit most likely explains partly, why CFIE CM is able to produce spurious free results.

Figure 19: Differences in current solutions at the internal resonance, $f \approx 131$ MHz: CFIE - MFIE on the left, CFIE - EFIE on the right.

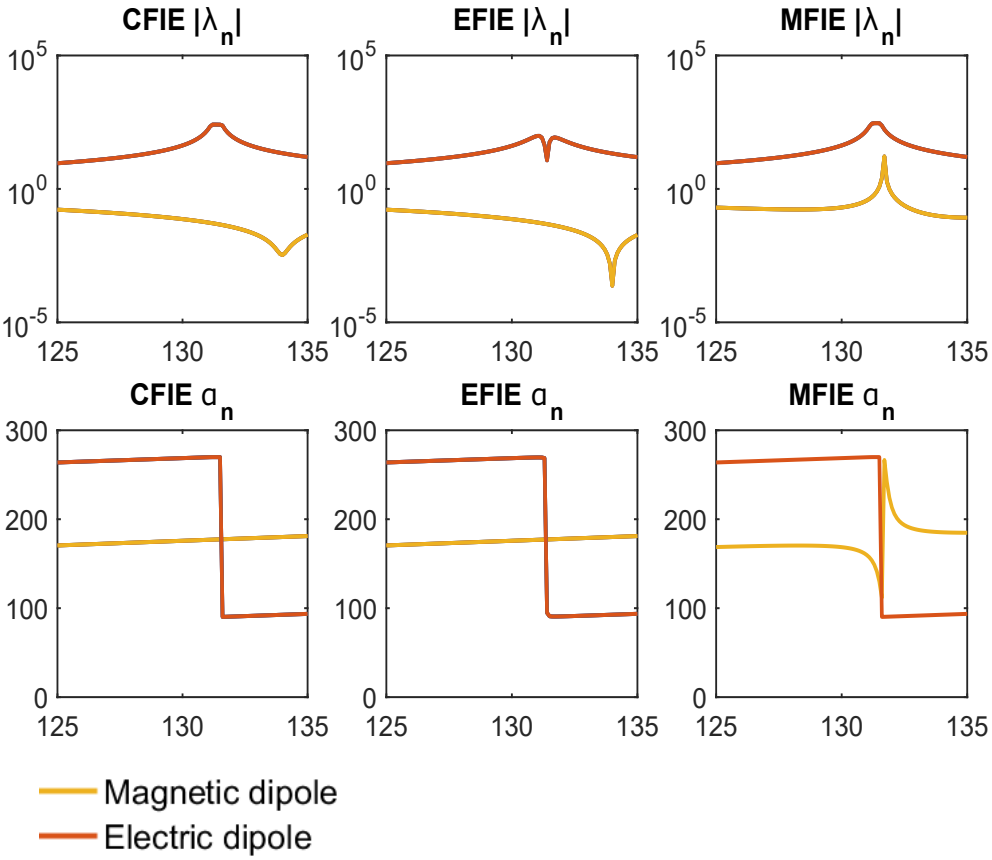

Figure 20: Eigenvalues (top) and -angles (bottom) as a function of frequecy [MHz] for the 1 m radius sphere with all three different formulations.

As can be seen in Figure 20, both EFIE and MFIE based modal solutions diverge from the CFIE based formulation. However they do so in different ways: EFIE seems to experience a diminishing eigenvalue, whereas for MFIE exactly the opposite is true. As the lower the eigenvalue for a mode, the more it contributes to the scattering for a proper excitation, it is only natural that the formulation experiencing increasing eigenvalues at its internal resonance receives worse results, as there a small error results to great relative error rather quickly.

Even if being an old topic, there is still quite a lot of discussion and dispute on the nature of internal resonances and thus further discussion is out of the scope of this work, however having taken quite a large deal of my time while trying to replicate and understand them. [25, 26] It is enough to know, that one should always be cautious when analysing scatterers composed of closed surfaces.

5.2 Plasmonic nanoparticles

If one is willing to formulate a new numerical scheme, it is of utmost importance to posses a proper benchmark for validation. Luckily for both PEC and penetrable objects, especially plasmonic ones, the Mie-expansions and its derivatives can and are widely used. [27]

Thus we begin by using the introduced TCM formulation on a 50 nm diameter silver sphere and compare it to an analytical MIE-solution, as done in Figure 21.

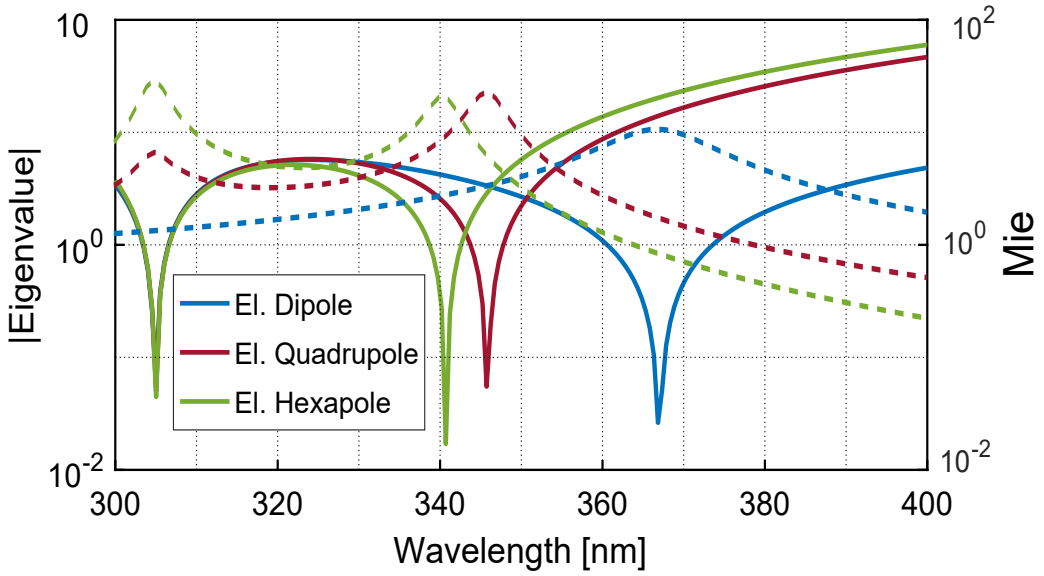

Figure 21: Eigenvalues (left axis, solid lines) and Mie-coefficients (right axis, dashed lines) for a 50 nm diameter silver sphere as a function of wavelength.

The absolute values of the Mie-coefficients aren't of utmost importance, but their extrema should describe resonances of corresponding modes, as seems to be the case

for this simple example. In Figure 21 the first 15 modes are plotted, but only three traces can be seen: this is, as already mentioned, TCM formulations are excitation independent and for a scatterer possessing such high spherical symmetry majority of the modes are practically similar in distribution but orthogonal in orientation. For instance there are three dipole modes, as shown in Figure 26, five quadrupoles etc., increasing in number with increasing modal number.

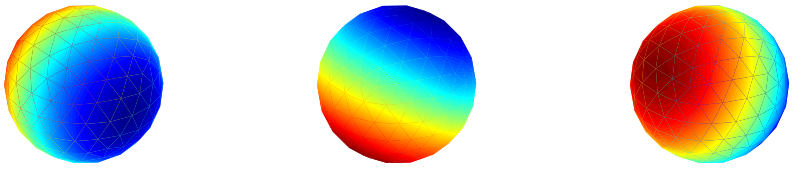

Figure 22: Three orthogonal dipole modes of a spherically symmetric object.

After validating the formulation, the usefulness of excitation independedness can be illustrated by breaking the symmetry of the scatterer under inspection. In Figure 23 an elongated silver rod 50 nm of length, cylindrical diameter of 5 nm with upper and lower spheroids of 5 nm is exposed to two plane waves of different propagation directions and polarizations. As can be expected due to the vast difference in electrical size or cross section, shadow, of the scatterer in different planes, the scatterers response is heavily dependent on the impinging excitation.

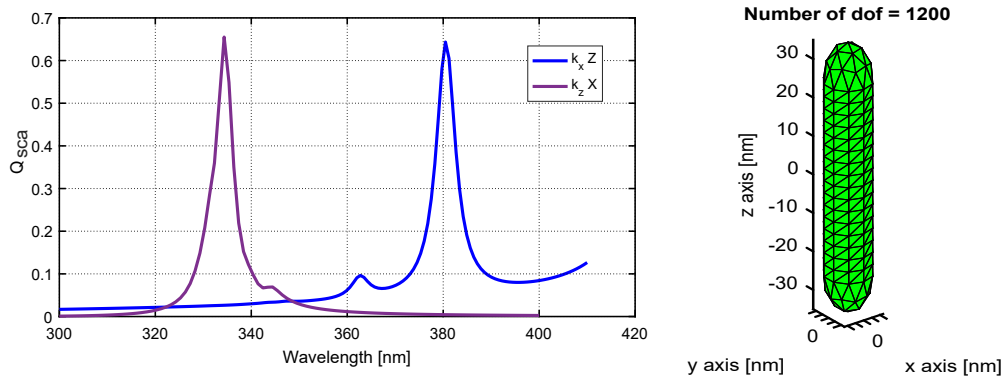

Figure 23: EM response of a 50 nm long silver rod for two differently polarized and oriented plane waves

Not always a plane wave is used to excite a scatterer, but for instance mobile phone PIFA-antennas rely heavily on near-field dipole excitations. As we expose our rod to a x-oriented dipole, we receive yet another response, shown in Figure 24. In this same Figure the first ten modes are plotted, already causing ten traces on the

plot. This is due to the already stated lack of symmetry compared to a sphere, which is further emphasized by the introduced modest in Figure 25. Each of the introduced excitations couples to different modes and thus produces a greatly varying response.

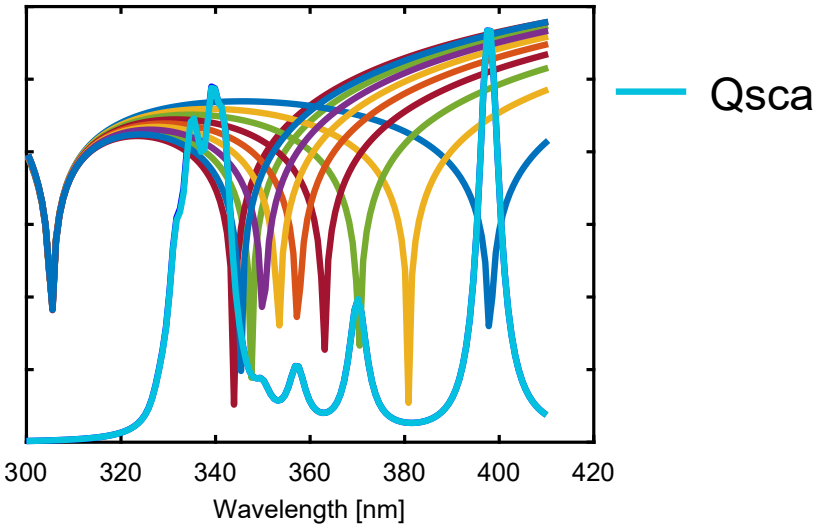

Figure 24: Modal analysis and scattering response (non-normalized) for the 50 nm long silver rod with. Scattering response is calculated with an x-oriented dipole near the rod.

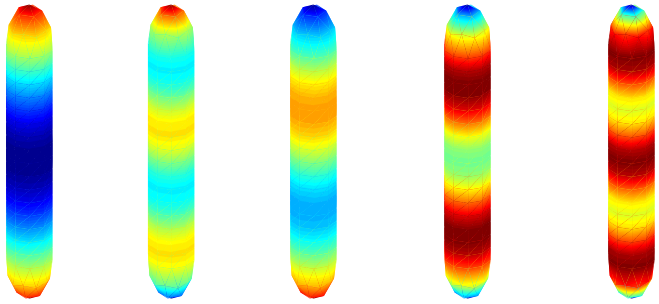

Figure 25: Five lowest order resonant modes for the 50 nm silver rod in the range from 300 to 410 nm.

In conclusion, as the EM response of a non-symmetric scatterer is heavily excitation dependent (polarisation, orientation, propagation direction), TCM offers a versatile, systematic, and thus a fast way for analysing scatterers, as the excitation dependence can be brought back to the solution via the already introduced modal expansion. Only mentioned in this work but not exploited, TCM can also be used for mutual coupling or polarisation related problems rather naturally due to the orthogonality properties of its modes and impedance-like representations.

Figure 26: Geometries used for validation of the new formulation: A 50 nm silver sphere with 15 (left) and 44 (right) nm air cores.

5.3 Core-shell structures

Here the new formulation in Equation (52) is validated. This is done yet again by comparing the results obtained through the formulation against the analytical Mie-like solution. In Figure 27 the results for a core-shell structure composed of a 50 nm silver sphere with a 15 nm spherical air core are compared. First of all, one should note, that the introduced formulation is able to accurately predict the location of the resonances. Secondly, when comparing to the Figure 21, the only effect caused by the core is a minor shift in the location of the resonances of the modes.

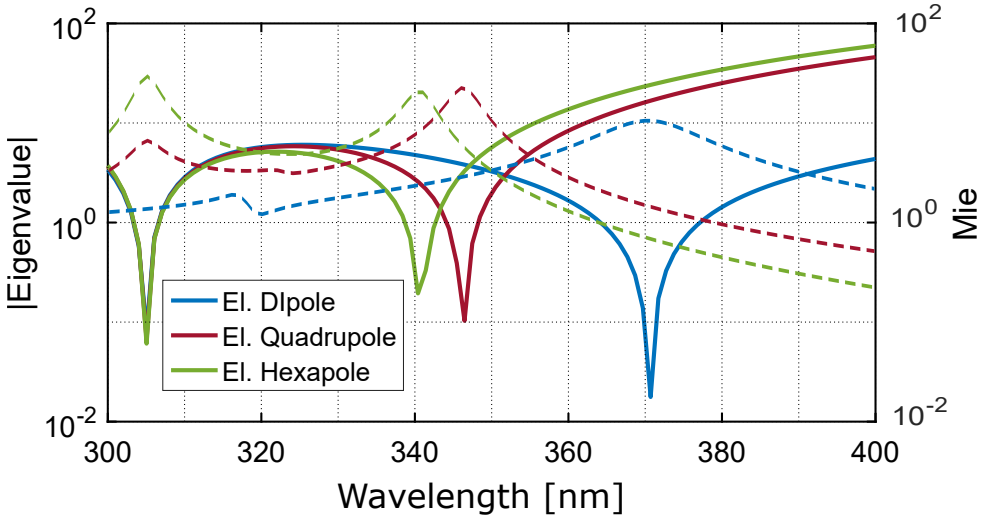

Figure 27: Eigenvalues (left axis, solid lines) and Mie-coefficients (right axis, dashed lines) for a 50 nm diameter silver sphere with a 15 nm air core as a function of wavelength.

The results for a larger air core of 44 nm inside the same 50 nm silver sphere

are shown in Figure 28. The obtained results are yet again in agreement with the Mie-theory, accurately describing the behaviour of even a couple of peculiarities: the main resonances of all the modes experience a red-shift, i.e, their resonant frequency lowers, whereas the singularity at which all modes resonate blue-shifts, i.e., its location increases in frequency.

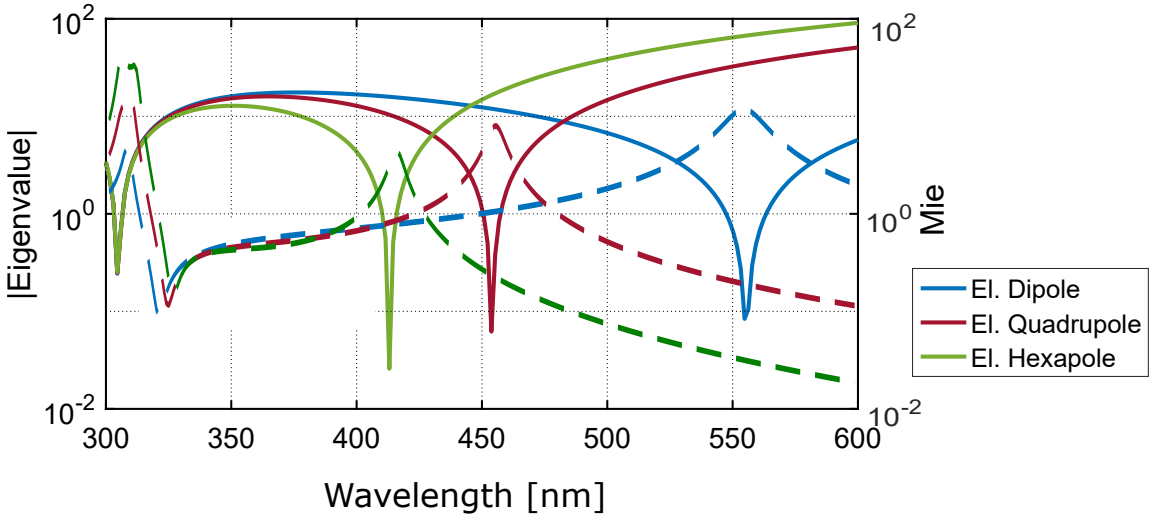

Figure 28: Eigenvalues (left axis, solid lines) and Mie-coefficients (right axis, dashed lines) for a 50 nm diameter silver sphere with a 44 nm air core as a function of wavelength.

Obtaining these results required rigorous mode tracking algorithms, as the amount of modes resonating approaches the level of our discretization and it was quite easy to lose track or mix up modes. Also, the location where all the modes resonate is near the point at which the permittivity obtained from the Drude model approaches zero. Even despite this our model seems to be able to accurately predict the behaviour of the scatterer under inspection. Thus it seems, that the introduced formulation is indeed valid for the characterization of multi-layered plasmonic scatterer.

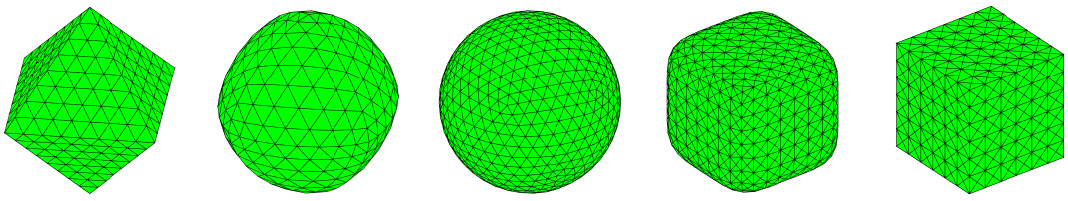

Figure 29: Superquadrics produced with $a = b = candr = s = t = p$, (from left to right) $p = 1, 1.5, 2, 5, \infty$.

The next step would be to study the responses obtained from quasi-canonical shapes, for instance *superquadrics*, illustrated in Figure 29. Superquadrics are a natural follow up, as they are quite well studied and can be described by a simple equation

$$\left|\frac{x}{a}\right|^r + \left|\frac{y}{b}\right|^s + \left|\frac{z}{c}\right|^t = 1 \tag{67}$$

where x, y and z are the cartesian coordinates, a, b and c describe the ellipticity along corresponding axis and the exponents r, s and t describe the major property of the surface, 1 meaning octahedron, 2 sphere and ∞ cube. [28]

As stated since the beginning, SIE solutions can be expanded back to the original 3D domain. In Figure 30 the radiation pattern of (one of the) dipole mode(s) is introduced, and it corresponds nicely to our our already introduced 2D cut and understanding of theory ("dipole doesn't radiate on its axis"). In Figure 31 then the E_{tan} tangential component of the received field solution is plotted, yet again resembling that of a classical dipole. Thus it seems, that for spherical scatterers with spherical cores the modes remain unchanged, at least for finite thickness's of shells, only their resonant frequency changing.

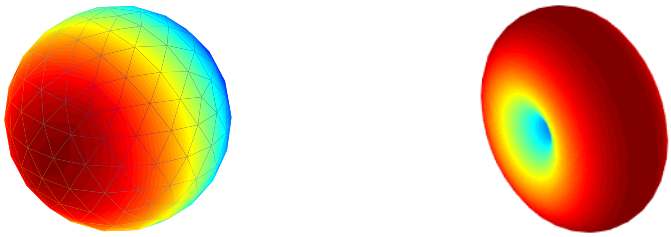

Figure 30: Dipole mode for 50 nm silver sphere with a 44 nm air core and its resulting radiation pattern.

After the geometries possessing well known singularities are studied and the accuracy of the method validated, they could and should be applied on even more complex structures like dielectric filled waveguides, MIMO antennas etc., where lot a of measurement results and rules of thumb exist, but additional systematic approach allowed by TCM would be a great benefit.

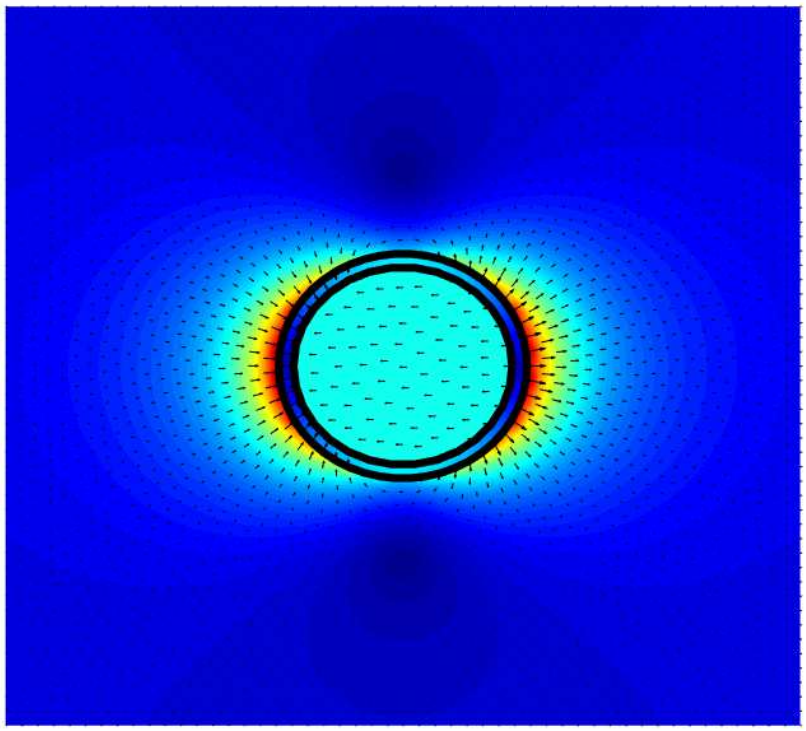

Figure 31: Near field solution, $\mathfrak{Re}(E_{tan})$ for the 50 nm silver sphere with a 44 nm air core on a 2D plane.

6 Conclusions

In this master's thesis, the electromagnetic characterization of scatterers via theory of characteristic modes was analysed. This was done by familiarizing the reader with the fundamental mathematical tools used in formulating a characteristic mode problem in a consistent and systematic way through surface equivalence principle/surface integral equations, allowing even the generation of a completely new formulation for multi-layered structures. The important properties and benefits of TCM are highlighted with numerical results and the new formulation is shown to be a success by comparing its results to well-known analytical solutions.

The numerical basis of surface integral equations were also introduced. Familiarizing myself with them, I noticed that even though well known, the problem of internal resonances is not completely solved nor even understood. This has already sparked a conference paper [25] and promising sketches for publications on the nature of resonances of conductors and especially penetrable objects.

Now that the new formulation has been shown to accurately describe modal properties of multi-layered scatterers, what is left is to study and design geometries not possessing closed form solutions. Especially the fields of plasmonics is quite interested in core-shell structures, which are but coated objects and thus can easily be studied with the introduced formulation. The new formulation can also be expanded quite linearly to n-layered structures.

This work has been organized such, that it is able to shed light on a topic that is considered to be rather abstract and thus avoided by many antenna engineers. Also I, the author of this work, had to familiarize myself with many mathematical tools, that used to be "black boxes" for me. Previously I hadn't used them to their full potential or even had used them completely wrong, resulting in non-physical and non-valid results. In this work I have shown my ability to device numerical formulations as well as evaluate their properties, arising from their mathematical and physical basis.

Last but not least it is worth noting that in this work only the surface of numerical methods were touched. For instance the impedance boundary condition was only introduced and the material was restricted to a rather simple one. However this work should be, in my humble opinion, a good start to more exquisite studies into surface integral equation representations and modal analysis of electromagnetic problems.

References

[1] Y. Chen and C.F Wang. *Characteristic modes: Theory and Applications in Antenna Engineering*. Wiley, 2015.

[2] P. Ylä-Oijala, S. P. Kiminki, H. Wallén, and A. Sihvola. Uniform surface integral equation formulation for mixed impedance boundary conditions. *IEEE Transactions on Antennas and Propagation*, 63(12):5718–5726, Dec 2015.

[3] S. A. Schelnukoff. Some equivalence tehorems of electromagnetics and their applications to radiation problems. *Bell System Technical Journal*, 15:92–112, 1936.

[4] M. Vollmer U. Kreibig. *Optical Properties of Metal Clusters*. Springer-Verlag Berlin Heidelberg, 1995.

[5] H. Wallén, H. Kettunen, and A. Sihvola. Composite near-field superlens design using mixing formulas and simulations. *Metamaterials*, 3(3-4):129–139, 2009.

[6] Y. Chang and R. Harrington. A surface formulation for characteristic modes of material bodies. *IEEE Transactions on Antennas and Propagation*, 25(6):789–795, Nov 1977.

[7] R. Harrington and J. Mautz. Computation of characteristic modes for conducting bodies. *IEEE Transactions on Antennas and Propagation*, 19(5):629–639, Sep 1971.

[8] R. Martens and D. Manteuffel. Systematic design method of a mobile multiple antenna system using the theory of characteristic modes. *IET Microwaves, Antennas Propagation*, 8(12):887–893, Sept 2014.

[9] M. Cabedo-Fabres, E. Antonino-Daviu, A. Valero-Nogueira, and M. F. Bataller. The theory of characteristic modes revisited: A contribution to the design of antennas for modern applications. *IEEE Antennas and Propagation Magazine*, 49(5):52–68, Oct 2007.

[10] J. Mautz and R. Harrington. A combined-source solution for radiation and scattering from a perfectly conducting body. *IEEE Transactions on Antennas and Propagation*, 27(4):445–454, Jul 1979.

[11] Q. I. Dai, Q. S. Liu, H. U. I. Gan, and W. C. Chew. Combined field integral equation-based theory of characteristic mode. *IEEE Transactions on Antennas and Propagation*, 63(9):3973–3981, Sept 2015.

[12] R. Harrington. Effects of antenna size on gain, bandwidth, and efficiency. *Nat'l Bureau of Standards*, 1960.

[13] G. Veronis and S. Fan. Modes of subwavelength plasmonic slot waveguides. *Journal of Lightwave Technology*, 25(9):2511–2521, Sept 2007.

[14] A. J. Poggio and E. K. Miller. Integral equation solutions of three-dimensional scattering propblems. *Computer Techniques for Electromagnetics, Chap. 4, Permagon, Elmsford, NY*, 1973.

[15] F. G. Hu and C. F. Wang. Integral equation formulations for characteristic modes of dielectric and magnetic bodies. *IEEE Transactions on Antennas and Propagation*, 64(11):4770–4776, Nov 2016.

[16] P. Ylä-Oijala, D. C. Tzarouchis, E. Raninen, and A. Sihvola. Characteristic mode analysis of plasmonic nanoantennas. *IEEE Transactions on Antennas and Propagation*, PP(99):1–1, 2017.

[17] S. Järvenpää, M. Taskinen, and P. Ylä-Oijala. Singularity subtraction technique for high-order polynomial vector basis functions on planar triangles. *IEEE Transactions on Antennas and Propagation*, 54(1):42–49, Jan 2006.

[18] K. Cools, F. P. Andriulli, D. De Zutter, and E. Michielssen. Accurate and conforming mixed discretization of the mfie. *IEEE Antennas and Wireless Propagation Letters*, 10:528–531, 2011.

[19] R. Harrington. *Field Computation by Moment Methods*. Macmillan, 1968.

[20] S. Rao, D. Wilton, and A. Glisson. Electromagnetic scattering by surfaces of arbitrary shape. *IEEE Transactions on Antennas and Propagation*, 30(3):409–418, May 1982.

[21] A. Buffa and S. H. Christiansen. A dual finite element complex on the barycentric refinement. *Comptes Rendus Mathematique*, 340(6):461 – 464, 2005.

[22] M. T. H. Reid and S. G. Johnson. Efficient computation of power, force, and torque in bem scattering calculations. *IEEE Transactions on Antennas and Propagation*, 63(8):3588–3598, Aug 2015.

[23] M. Taskinen P. Ylä-Oijala and J. Sarvas. Surface integral equation method for general composite metallic and dielectric structures with junctions. *Progress in Electromagnetic Research*, 42:81–108, 2005.

[24] S. Järvenpää P. Ylä-Oijala, J. Markkanen and S. P. Kiminki. Surface and volume integral equation methods for time-harmonic solutions of maxwell's equations. *Progress in Electromagnetic Research*, 149:15–44, 2014.

[25] P. Ylä-Oijala, J. Lappalainen, D. Tzarouchis, and A. Sihvola. On the resonances of characteristic modes. In *32nd URSI GASS, Montreal*, 2017.

[26] T. K. Sarkar, E. L. Mokole, and M. Salazar-Palma. An expose on internal resonance, external resonance, and characteristic modes. *IEEE Transactions on Antennas and Propagation*, 64(11):4695–4702, Nov 2016.

[27] M. Gustav. Beiträge zur optik trüber medien, speziell kolloidaler metallösungen. *Annalen der Physik*, 330(3):377–445, 1908.

[28] D. Tzarouchis, P. Ylä-Oijala, T. Ala-Nissila, and A. Sihvola. Shape effects on surface plasmons in spherical, cubic, and rod shaped silver nano-particles. *Applied Physics A, Vol. 122, No. 4, paper 298 (7 pages)*, 2016.